HISTONE ACETYLATION LANDSCAPE IN *S. cerevisiae nhp6ab* MUTANTS REFLECTS ALTERED GLUCOSE METABOLISM.

Durano Diletta[a,1], Di Felice Francesca[a,1], Caldarelli Federica[a], Lukacs Andrea[a], D'Alfonso Anna[a], Saliola Michele[a], Sciubba Fabio[b], Miccheli Alfredo[b], Zambelli Federico[c], Pavesi Giulio[c], Bianchi Marco Emilio[d] and Camilloni Giorgio*[a,e,f] (giorgio.camilloni@uniroma1.it)

(1) these authors equally contributed to this work

a) Dipartimento di Biologia e Biotecnologie, Sapienza Università di Roma. Rome, Italy

b) Dipartimento di Chimica, Sapienza Università di Roma, Rome, Italy

c) Dipartimento di Bioscienze, Università di Milano, Milan, Italy

d) Chromatin Dynamics Unit, IRCCS San Raffaele Scientific Institute and San Raffaele University, Milan, Italy

e) Istituto di Biologia e Patologia Molecolari, CNR, Rome, Italy

f) Dipartimento di Biologia e Biotecnologie, Sapienza Università di Roma, Laboratory affiliated to Istituto Pasteur Italia – Fondazione Cenci Bolognetti

*Corresponding author - E-mail: giorgio.camilloni@uniroma1.it

tel: +390649912808; Fax +390649912500

ORCID: 0000-0002-1195-6142

Dipartimento di Biologia e Biotecnologie, Sapienza Università di Roma. Piazzale A. Moro 5, 00185 Rome, Italy

Abstract

BACKGROUND

The execution of many genetic programs, influenced by environmental conditions, is epigenetically controlled. Thus, small molecules of the intermediate metabolism being precursors of most of nutrition-deriving epigenetic modifications, sense the cell surrounding environment.

METHODS

Here we describe histone H4K16 acetylation distribution in S. cerevisiae nhp6ab mutant, using ChIP-seq analysis; its transcription profile by RNA-seq and its metabolic features by studying the metabolome. We then intersected these three -omic approaches to unveil common crosspoints (if any).

RESULTS

In the nhp6ab mutant, the glucose metabolism is switched to pathways leading to Acetyl-CoA synthesis. These enhanced pathways could lead to histone hyperacetylation altering RNA transcription, particularly of those metabolic genes that maintain high Acetyl-CoA availability.

CONCLUSIONS

Thus, the absence of chromatin regulators like Nhp6 A and B, interferes with a regulative circular mechanism where histone modification, transcription and metabolism influence each other and contribute to clarify the more general phenomenon in which gene regulation feeds metabolic alterations on epigenetic basis.

GENERAL SIGNIFICANCE

This study allowed us to identify, in these two factors, a common element of regulation in metabolism and chromatin acetylation state that could represent a powerful tool to find out relationships existing between metabolism and gene expression in more complex systems.

Keywords: chromatin; epigenetics; yeast; transcriptome; metabolome

1. INTRODUCTION

Chromatin is the complex functional structure in which DNA and histone and non-histone proteins are organized. This complex organization allows the whole DNA to be restrained and accommodated within the small nuclear compartment in orderly manner and contributes to the differential expression of the genes it hosts. The histone content of the cell

nuclei, a parameter so far considered fixed as well as the cell DNA content, is conversely quite variable depending on the cellular conditions [1, 2], or on the mutation of specific genes [3,4]. Consequences of a reduced amount of histone proteins have been reported as: reduced genome stability, reduced cellular proliferation and premature ageing. *S. cerevisiae* Nhp6a and Nhp6b proteins (93 and 99 aminoacids long respectively), belong to the HMG-Box family [5], and contribute to the maintenance of the proper histone protein amount inside the cell [4]. These two proteins are considered highly redundant in their functions, even though interesting differences have been reported [6]. The genome-wide distribution of Nhp6a protein shows it is widespread in the chromosomes although specific positions have been observed [7]. Lacking of both Nhp6 proteins has been associated to a reduced histone amount and to a different genome-wide nucleosome occupancy [4], as well as to altered transcriptional and translational profiles of histone genes [8]. In fact *nhp6ab* double mutants show rDNA hyperacetylation particularly of the H4K16 residue [9].

Chromatin acetylation state is strongly influenced by the metabolic pathway utilized by the cells and this is also true for other epigenetic mechanisms of regulation [10]. Since effectors of these latter are products of intermediate metabolism (i.e. S-Ade-Met for DNA and histone methylation, Acetyl-CoA for protein acetylation and NAD+ for sirtuin activities), it is conceivable to hypothesize that metabolic alterations arising from nutrient availability or defects in metabolic processes, lead to altered amounts of these substances inside the cells. This directly may affect the epigenetic modifications and, in turn, gene expression [11]. Moreover, nucleosome positioning and abundance in a given genetic locus of the genome also represent a further level of epigenetic control [12]. Given the ATP-dependence of all the "remodeling machineries" responsible for nucleosome rearrangements, also energy availability links remodeling processes to metabolism [13]. In this context, Acetyl-CoA plays a pivotal role being a polyfunctional molecule because while sensing nutrients availability it can be considered as an energetic fuel for the cell. In fact, Acetyl-CoA is the end-product of glucose metabolism and is also the activated compound responsible for acetylation. Glucose, through a complex network of transducing signals common to all eukaryotic cells, fuels this compound into the energy necessary for ATP biogenesis. Glucose is converted into two pyruvate molecules via sequential glycolitic steps. In yeast two major routes convert pyruvate into Acetyl-CoA: the cytoplasmic pyruvate dehydrogenase bypass activated by the *PDC1*, *PDC5* and *PDC6* gene products and the mitochondrial pyruvate dehydrogenase complex of the Krebs cycle.

Given the *nhp6ab* mutant hyperacetylation phenotype at rDNA locus, we extended this observation genome-wide. Data obtained have been compared to transcriptomic and metabolomic results in order to shed light on causal link with each other.

2. MATERIALS AND METHODS

2.1 Yeast strains used in this work

WT - *Mat α; ura3-52; trp1-289; his3-Δ1; leu2 3112; gal2; gal10*

nhp6ab - *Mat α; ura3-52; trp1-289; his3-Δ1; leu2 3112; gal2; gal10; nhp6a-Δ3::URA3; nhp6b-Δ3::HIS3*

pot1 - *Mat α; ura 3-52; trp 1-289; his 3- Δ1; leu 2-3, 112; gal2; gal10; pot1::KAN*

pot1/nhp6ab - *Mat α; ura 3-52; trp 1-289; his 3-Δ1; leu 2-3, 112; gal2; gal10; nhp6a-Δ3::URA3; nhp6b-Δ3::HIS3; pot1::KAN*

2.2 Oligonucleotides

ACS1f 5' CCGCAATTGCTACCCACTAT

ACS1r 5' GTTTAATTGGCCGTTGAGGA

ACS2f 5' TGCTAATCCCGACAAGCCAG

ACS2r 5' AATACGAGCCACAGCCAACA

PDA1f 5' TGAGACTTCGAAAGCCACCT

PDA1r 5' CATTCTCGATACCGACAGCA

POT1f 5' GGTCCGTAGCCAACCAGTTA

POT1r 5' CCGCGAATGCTTCATTTATT

UBC6f 5' GATACTTGGAATCCTGGCTGGTCT

UBC6r 5' AAGGGTCTTCTGTTTCATCACCTG

2.3 Culture media and conditions

Yeast cultures were grown and manipulated according to standard protocols [14]. YPD medium (1% bacto yeast extract, 2% bacto peptone, 2% glucose) was used for all strains. H_2O_2 treatments: cells were grown in YPD medium supplemented with 3mM H_2O_2 (30' min). Then serial threefold dilutions were spotted on YPD plates.

2.4 Protein analysis

Proteins were extracted, by vigorous shaking for 1 h at 4°C, using NP40 buffer (0.2% NP40, 200 mM NaCl, 50 mM Tris pH 7.5, 1 mM PMSF, and protease inhibitors) and glass beads (Sigma-Aldrich, G9268-500G). 15 µg of protein extract were subjected to PAGE using pre-cast gel Mini-PROTEAN TGX Stain-Free BIORAD and transferred on nitrocellulose membrane. Overnight incubation with primary antibodies was performed at 4°C. Primary antibodies used: anti rabbit histone H3 (C-terminus domain) (H3Ct) (Abcam) at 1:1000 dilution; rabbit anti-acetyl-H4 at 1:1000 dilution (Upstate/Millipore); rabbit anti-acetyl H4K16 at 1:2000 (Santa Cruz Biotechnology); rabbit anti-acetyl H3 at 1:2000 (Upstate/Millipore). Secondary antibody: anti-rabbit IgG-HRP (Jackson ImmunoResearch) at 1:15000 dilution. Detection was obtained by SuperSignal West Pico Chemiluminescent Substrate (Thermo Scientific) staining. Quantification of bands was performed using ImageJ 1.42q software. H3Ct signals were used to normalize histone acetylation values.

2. 5 Libraries construction and Illumina Sequencing for ChIP-seq and RNA seq analysis.

2.5.1 ChIP-seq: 100ng of IP and Input DNA from WT and *nhp6ab*, each in duplicate from different cell cultures, were subjected to first quality control with Bioanalizer. Next, NuGEN's Ovation Ultralow DR Multiplex System kit was used for generating non-cohesive ends (end-repair) and for ligation of barcode adapters for multiplexing. Finally, DNA libraries were generated through PCR and subjected to quality control (profile evaluation, concentration estimate, whether or not the adapters were checked) with the selection of fragments populations in a smaller range of sizes. Starting from these libraries, amplification of the clusters were generated using Bridge PCR technology inside the cBot Illumina. Sequencing was performed by means of a HiSeq 2000 Illumina and raw base files were processed through the HiSeq 2000 CASAVA pipeline for primary analysis. The base call accuracy is determined by the Phred Quality Score (Q score) which indicates the probability for a given base to be incorrectly called by the sequencer: Q = -10 log10P.

2.5.2 RNA-seq: 100ng of RNA from each sample (in duplicate) from WT and *nhp6ab* were retrotranscribed. Resulting cDNAs were processed as reported above for ChIP-seq procedure.

2.6 ChIP analysis was performed as previously described [9]. Briefly: 350 μg of chromatin extract were incubated overnight with the following primary antibodies: anti-H4K16Ac and anti-H4 (Santa Cruz Biotechnology). Protein A Sepharose beads (Amersham, GE Healthcare) allowed to recover chromatin-antibody complexes by 1.5 h incubation at 4°C on a rotating wheel. Purified DNA was processed for library preparation for ChIP-seq analysis.

2.7 RT qPCR

RNA was extracted from exponentially yeast growing cells (OD600 0.5/ml) as previously described [15]. RNA samples (1.5 μg), DNase reacted, were subjected to retro-transcription with 2.5 μM oligo-dT and incubated with 50U Bioscript Reverse Transcriptase (Bioline) for 1h at 42°C. The reaction was stopped by heating at 85°C for 5 min, then samples were chilled on ice. cDNA amplification was performed (triplicate) for each sample, employing Sso Advanced SYBR Green supermix (Bio-Rad) in a Mini Opticon Real-time PCR System (Bio- Rad). The values obtained (at least three independent experiments) were normalized to those of UBC6 [16].

2.8 Bioinformatic analysis of sequencing data

2.8.1 ChIP-Seq data. Quality control of sequence reads was performed with FastQc, that revealed a global decrease in quality of base calling in the last 5 bp of the reads. Thus, reads were manually trimmed by 5 bp at the 3' end, and mapped on the yeast genome (Saccharomyces cerevisiae S288c – April 2011 assembly) with Bowtie [17].Trimmed reads were required to map completely on the genome with at most two substitutions. Mappings of the two replicate experiments of both WT and nhp6ab were merged for subsequent analyses.

To compute ChIP-Seq read enrichment in nucleosome regions returned by MNase-Seq, and accommodate for differences in resolution due to the different fragmentation protocols of the two assays, reads mapped on the genome

were first shifted by 100bp in the 5'->3' direction on the respective strand. Raw read counts in each nucleosome region were computed by considering the resulting 5' positions on the genome of the shifted reads. Coordinates of nucleosome regions were retrieved from 4. A nucleosome in WT was considered to be overlapping with a nucleosome in nhp6ab if at least 75% of its base pairs were covered by a nucleosome in nhp6ab, and vice versa the 75% of the base pairs of the nhp6ab nucleosome covered by the WT nucleosome region. The resulting pairs of nucleosomes with mutual overlap of at least 75%, were considered "common" between WT and nhp6ab, while the remaining ones defined as WT- or mutant-specific, respectively. Enrichment of WT and mutant ChIP experiments on nucleosomes was defined for each nucleosome region "i" as Reads per Million per Kilobase of Nucleosome as follows: $RMKNi=Ci/N \bullet Bi \bullet 10^9$

where Ci is the raw count of shifted reads in WT or mutant in the nucleosome region, Bi is the size in base pairs of the nucleosome region as retrieved from [4], and N is the total number of reads of the ChIP-Seq (either WT or mutant) mapping on all the nucleosome regions.

2.8.2 RNA-Seq . Rsem [18] with default parameters was employed to map sequence reads on ORF sequences of yeast gene annotation sacCer3, producing the subsequent read counts for each ORF. Counts of the two replicates for WT and the two for nhp6ab showed excellent concordance, respectively, assessed both by Pearson correlation on read counts ($r > .99$) and principal component analysis (PCA, data not shown). Similar results, with little or no dispersion of expression values (read counts) across replicates, were already available in literature in an experimental context analogous to the one of this work [19]. Thus, we deemed two replicates to be sufficient for obtaining reliable results from subsequent analyses. Differential expression analysis was performed on the resulting read counts with DESeq2 [20], with default parameters. Differentially expressed genes were selected as having 1) a FDR associated with expression change by DESeq2 lower than 0.01 and 2) having a log2-fold ratio change of expression between WT and mutant greater than 1.5 (upregulated) or lower than -1.5 (downregulated). Gene ontology functional enrichment analysis was performed with the Gene Ontology Term Finder tool available at the Saccharomyces Genome Database [21].

Sequencing data discussed in this publication have been deposited in NCBI's Gene Expression Omnibus [22] and are accessible through GEO Series accession number GSE108219.

2.9 Metabolome analysis

2.9.1 Cellular quenching and extraction procedure.

Yeast cells were grown to the exponential phase and 1g of wet WT and *nhp6ab* cells were collected. Cells were washed twice with cold PBS. 2 ml of methanol and 1 volume of glass beads were added. The cells were lysed by vigorous shaking for 1 h at 4°C. Samples were centrifuged and the supernatants recovered. Each sample was mixed with 2 ml of chloroform and 2 ml of water and incubated over night at 4°C. The next day the samples were centrifuged and the aqueous phase was collected, dried under N_2 and stored at −80 °C until NMR analysis [23, 24].

2.9.2 Sample preparation for NMR analysis. The freeze-dried amples were re-dissolved in 600 μL of D_2O phosphate buffer solution (pH=7.4) containing 2mM sodium 3-(trimethylsilyl) propionate-2,2,3,3-d4 (TSP) as 1H NMR reference, and transferred to 5mm NMR glass tubes for analysis. 600 μL of culture media were collected at the beginning and at the end of experimental intervals and stored at −80 °C until NMR analysis. 60 μL of a D_2O solution containing 20 mM sodium 3-(trimethylsilyl) propionate-2,2,3,3-d4 (TSP) were added to the sample as 1H NMR internal reference. Data were expressed as differences between the levels at the end of the experimental time and at the beginning of the culture. The values obtained are representative of net balances, with positive and negative values being considered an estimate of net fluxes of production and utilization of metabolites, respectively, as previously reported [25, 26].

2.9.3 NMR spectroscopy

1H NMR spectra were acquired at 25°C using a Bruker Avance III 400 spectrometer (Bruker BioSpin GmbH, Germany) equipped with a magnet operating at 9.4 Tesla, where the 1H nucleus resonates at 400.13 MHz. The probe-head was a 5 mm diameter multinuclear PABBO BB-1H/D (Z108618/0044) equipped with z-gradient.

The pulse sequence adopted for spectra acquisition was a presaturation–single 90° detection pulse–acquire–delay sequence where the D1 relaxation delay was optimised to 2.5 s to allow the acquisition of 64k data point in about 5.5s, satisfying full relaxation conditions.

The length of the detection pulse was calibrated previously to the acquisition of each spectrum, the spectral width was set to 6009.62Hz (15 ppm) and 64 scans were collected for each spectrum.

2.9.4 Data analysis

1H NMR spectra were processed using the 1D-NMR Manager ver. 12.0 software (Advanced Chemistry Development, Inc., Toronto, Ontario, Canada). The assignment of the peaks to specific metabolites was achieved by standard two-dimensional (2D)1H-1H total correlation spectroscopy(TOCSY), 1H-13C heteronuclear single quantum correlation (HSQC), and heteronuclear multiple bond correlation (HMBC) and confirmed using an internal library of compounds, literature data and HMDB database [27, 28].

The acquired NMR spectra were manually phased and baseline corrected; polar spectra were referenced to the chemical shift of the TSP methyl resonance at δ 0.00 ppm.

The quantification of metabolites was obtained by comparison of the integrals of specific signals to the internal standard (TSP) integral. BMRB accession number 27871

3. RESULTS

3.1 Increased and widespread distribution of H4K16 acetylation in *nhp6ab* mutant.

We have previously reported *S. cerevisiae nhp6ab* mutant profound epigenetic alterations: reduced histone protein content, global altered nucleosomal occupancy and a hyperacetylated H4K16 phenotype of the rDNA locus [4,8]. We asked whether the increased H4K16 acetylation phenotype is limited to the rDNA locus or if it could be extended to other regions. To evaluate the overall increase in H4K16 acetylation we performed immunoblotting experiments with antibodies against H4K16Ac. Results reported in Figure 1 confirmed a significant increase of the total H4K16Ac amount in the *nhp6ab* mutant cells compared to WT, together with the expected reduction of H3 protein.

We then used the Chromatin Immunoprecipitation (ChIP) followed by High Throughput sequencing (ChIP-seq) to study the distribution of this histone modification in all the 16 *S. cerevisiae* chromosomes. Results reported in Figure 2 (as a sample of all chromosomes), concerning chromosomes IV, XII and XIII, show a widely distributed hyperacetylation of the mutant strain higher if compared to the WT, and this is true for all chromosomes [NOT SHOWN]. A definitive strategy or pipeline for the identification of differential enrichments in the comparison of ChIP-seq experiments has not been established [29]. A major issue is how to normalize the read counts across the ChIP-seq experiments to be compared and also how to define the genomic regions on which the comparison has to be performed, in order to point out differentially enriched loci. To assess differential enrichments for H4K16Ac we took advantage of the previously reported nucleosome occupancy data (MNase-seq) available for both strains [4]. This information provided a straightforward solution for both the aforementioned issues. Read counts in each experiment were normalized according to the overall count of reads contained only in genomic regions occupied by nucleosomes as defined by MNase-seq that is regions where histone modifications should occur. WT ChIP-Seq was normalized according to reads within WT MNase-seq nucleosome regions, likewise *nhp6ab* was compared to the corresponding *nhp6ab* MNase-seq experiment. Differential enrichment was then assessed separately on each nucleosome associated region in either condition, by comparing the normalized read counts obtained from WT and *nhp6ab* ChIP-Seqs..

Figure 3A shows the distribution of IP read counts normalized as just described and defined as "reads per million per kilobase per nucleosome" (RMKN, see methods). RMKN is significantly higher in *nhp6ab* mutant relative to WT (“all”, in Figure 3A), since H4 is more acetylated and fewer histones are present. We then stratified enrichment of "specific" or “common” nucleosomes. To accommodate for experimental variability in the definition of nucleosome coordinates through MNase-seq, we defined as “common” nucleosomes between WT and *nhp6ab* those that had a reciprocal overlap of at least 75% of the nucleosome associated region. Nucleosomes with <75% overlap were defined as WT- or *nhp6ab* specific. Interestingly, nucleosomes from *nhp6ab* strain show increased acetylation regardless of being "specific" or "common" in all the performed comparisons (Figure 3a).

In *S. cerevisiae*, H4K16 acetylation is mainly associated to transcriptional activation [30], even if its involvement in both activating and suppressing transcriptional silencing has been reported [31]. In order to test whether increased

H4K16 acetylation in the *nhp6ab* strain is associated with a transcriptional up regulation, we took advantage of available microarray data [4] indicating an altered transcription profile in *nhp6ab* cells, and we then employed RNA-seq (quantifying PolyA$^+$ RNAs from WT and *nhp6ab* cells) to produce to a new transcriptome quantification to be superimposed on our ChIP-seq data concerning H4K16Ac. Consistently with microarray data [4] , the overall distribution of transcript levels shows a globally increased gene expression in *nhp6ab* mutant (Figure 3B, plot Transcript per million WT vs *nhp6ab*).

The superimposition of RNA-seq data with those from ChIP-seq and MNase-seq [4] allowed us to correlate chromatin acetylation state and nucleosome occupancy also in transcribed regions. The latter have been further distinguished as up-regulated and down-regulated according to the results of the RNA-Seq analysis. Although ChIP and Mnase data rely on different techniques for DNA fragmentation, both approaches provide reliable and comparable results. Thus we could assess relationships between chromatin organization and nucleosome occupancy (Mnase profiles), and between histone modifications (ChIP seq) and transcription (RNA-seq).

The comparisons allowed us to highlight that nucleosome-protected regions are more acetylated in the mutant respect to the WT. Similarly nucleosomes located in transcribed regions seem to be more acetylated in the mutant than in the WT, with a more marked difference for nucleosomes localized within up-regulated genes (Figure 3C). Since Gene Ontology (GO) enrichment analysis performed on microarray data by Celona and colleagues indicated a marked transcriptional deregulation of metabolic genes [4], we employed the same approach on genes resulting differentially expressed in our RNA-seq data. The GO analysis (Table 1) indeed showed that, among different "biological processes" the most deregulated categories are those involved in metabolic processes (with 28/36 down-regulated categories and 7/13 up-regulated, all highlighted in yellow). These results are completely in agreement with those returned from the microarray-based analysis previously reported [4].

3.2 Matabolite profile in WT and *nhp6ab* cells by 1H-NMR spectroscopy

According to the GO analysis derived from RNA-seq, we further investigated in detail the *nhp6ab* metabolic state. We performed a metabolomic analysis by 1H NMR spectroscopy. We profiled aqueous extract phases from cells exponentially growing on glucose, as well as their culture medium, as specified in materials and methods. The medium was used to calculate the external metabolite balances (before and after growth).

S1 Table reports the resonance assignments of the metabolites present in cell extracts and in culture medium.

S2 Table reports the intracellular metabolite concentrations expressed as μmol/g wet weight of cells. Fig 4 reports the medium metabolite changes, expressed as a net balance of concentration (mM) between the cell and the medium. The sign of the net balance indicates the direction of change: the positive sign indicates excretion of the metabolite from the

cells; the negative one indicates an influx inside the cell. *nhp6ab* mutant cells show a trend of higher uptake of amino acids, trealose and glucose, fumarate and lactate, but a lower production of ethanol and formate. Glutamate and lysine levels did not vary significantly, and histidine and glycine levels were significantly lower in *nhp6ab* cells (S2 Table).

Absolute differences in metabolite intracellular levels between *nhp6ab* and WT cells were then examined. No significant differences were observed for acetate, succinate, fumarate and formate. Pyrimidine nucleotides, such as UTP, UDP and UMP, were higher in *nhp6ab* cells, while ATP+ADP levels were lower (S2 Table). Finally, NAD^+ levels were not different between the two strains, although glutathione levels were higher and nicotinamide riboside levels, a metabolic intermediate of NAD^+ salvage pathway, were significantly lower in *nhp6ab* cells.

Overall, these results indicate a sharp alteration of metabolic state in *nhp6ab* cells, both as different steady state levels of metabolites, and fluxes. In particular, increased glutamate uptake in *nhp6ab* cells with no change in its steady-state level might be a consequence of an increased glutathione and glutamine synthesis (whose levels increased), as well as toward TCA cycle intermediates.

3.3 Drawing *nhp6ab* metabolic pathways by metabolomic and transcriptomic data

To better characterize the metabolic state of the *nhp6ab* mutant, we wanted to compare the different metabolic pathways from the WT and from the mutant strain as depicted by -omic data. Even if each involved enzyme was not directly and quantitatively measured, a comparison between the expression level of genes by which they are encoded (RNA-seq) and key metabolites produced by their activities (metabolome) can represent a useful strategy to make a prevision about the employment of the main metabolisms. Differentially expressed genes list (S5_table) is available in supplementary material. Thus, we could find alterations on the following pathways:

1. FIRST PART OF GLYCOLYSIS: FROM GLUCOSE TO GLYCERALDEHYDE 3-P (Pathway 1 in Figure 5)

Transcriptome analysis showed that some of the various genes involved in the first glycolysis steps are over-expressed in the mutant with respect to the WT, in particular *PGI1* and *FBP1*. These results have suggested that in the mutant strain there's a sort of "funnel" along the glycolytic pathway, the consequence of which is the accumulation of Fructose 6-P and Glucose 6-P.

2. PENTOSE PHOSPHATE PATHWAY (Pathway 2 in Figure 5)

The Pentose Phosphate pathway, powered by Glucose 6-P, produces Glyceraldehyde 3-P. A significant increase in the various genes involved (red arrows in the figure) emerged in the *nhp6ab* mutant strain compared to WT. This metabolic pathway involves the reduction of 2 $NADP^+$ molecules to NADPH. The accumulation of this cofactor is evidenced by the presence of the dimeric form of G6PDH, distinct in native PAGE from the tetrameric form (Figure S1). The fast migrating G6PDH activity band is a dimeric form of the enzyme, produced by the inhibitory effect of NAPDH

accumulation [32]. Furthermore, being the NADPH accumulation toxic for the cell [33] we verified whether, in the mutant strain, other metabolic pathways were activated that could guarantee its re-oxidation to $NADP^+$. The transcriptome analysis provided us an over-expression of the *GLR1* gene (Glutathione Reductase NADPH-dependent) responsible for the passage of Glutathione from the oxidized form (GSSG) to the reduced one (GSH) (Pathway 3 in Figure 5).

The transcriptome analysis showed an increase in *TPI1* gene expression, responsible for the conversion of Glyceraldehyde 3-P into Dihydroxyacetone-P (DHAP). This molecule, in turn, undergoes spontaneous conversion into Methylglyoxal, which is also remarkably toxic to the cell [34]. Methylglyoxal is further transformed into lactate using reduced glutathione (GSH, which is provided by the *GLR1* gene above described). The following involvement of *GLO2* and *GLO4* genes (for which over-expression has been observed in the mutant) provides oxidized glutathione (GSSG) again. The use of this pathway is confirmed by the increased amount of lactate found with the metabolomic approach in the *nhp6ab* mutant (see Table S2).

The Pentose Phosphate pathway also provides appropriate levels of Ribulose 5-P and therefore of 5-phosphoribosil 1-pyrophosphate (PRPP) both involved not only in the synthesis of nucleotides but also in that of amino acids, in some recycling and in the formation of NAD^+ and $NADP^+$ (Figure 5, Pathway 4, not detailed).

Metabolome analysis also provides clues of the Pentose Phosphate pathway preferential employment by the mutant strain, since it shows an increase in purines and pyrimidines presence inside the mutant cells compared to those of the WT strain.

The preferential (and probably obligatory) use of these metabolic alternative pathways instead of the glycolytic one undertaken by the *nhp6ab* mutant can be further evidenced by the intracellular accumulation of glucose, highlighted by the metabolomic analysis. The glucose that is not oxidized along the glycolytic pathway triggers the futile cycle of Trehalose which accumulates in turn. The genes involved in the futile cycle of trehalose are in fact up regulated in the mutant (Red Arrows, Pathway 5 in Figure 5).

4. GLYCEROPHOSPHOLIPIDS BIOSYNTHESIS (Pathway 6 in Figure 5)

The DHAP deriving from the Glyceraldehyde 3-P thanks to *TPI1* gene product can undertake three ways:

1. Conversion in Methylglyoxal (just described)

2. Conversion into Glycerol 3-P thanks to the intervention of *GPD1*, *GPD2* (glycerol 3-P dehydrogenase NAD^+-dependent), and *GUT2* (mitochondrial glycerol 3-P dehydrogenase). Glycerol 3-P can accept an acyl group and transform into 1-Acyl-sn-glycerol 3-P by the action of the *SCT1* and *GPT2* gene products.

3. Conversion of DHAP to 1-Acyl-DHAP thanks to the intervention of *SCT1* and *GPT2*. The 1-Acyl-DHAP is converted into 1-Acyl-sn-glycerol 3-P by the NADPH-dependent DHAP reductase gene *AYR1*.

The genes involved in the convertions from 2 to 3 are all over-expressed in the mutant with respect to the WT.

The 1-Acyl-glycerol 3-P thus produced is transformed into triacylglycerol through successive reactions involving genes mostly over-expressed in the mutant. Each of the intermediate acylation products (1-sn acyl, 1,2-diacyl, tri-acyl) is a source of fatty acid molecules catalyzed by the products of the *TGL2*, 3 and 4 genes, all upregulated in the mutant.

5. SECOND PART OF GLYCOLYSIS: FROM GLYCERALDEHYDE 3-P TO PYRUVATE (Pathway 7 in Figure 5)

In yeast cells that use glucose as fermentable carbon source, most of the Glyceraldehyde 3-P derives from glycolysis (pathway1), the final product of which is pyruvate. Transcriptome analysis has highlighted that the *nhp6ab* mutant strain preferentially uses the Penthose Phosphate pathway (pathway 2), as witnessed in native PAGE by the accumulation of dimeric form of G6PDH ((Figure S1). Thus, in *nhp6ab* mutant cells the glyceraldehyde 3-P comes mainly from penthose phosphate pathway and in lesser quantity from glycolysis. Nevertheless genes involved in these transformations emerge to be equally expressed in the two strains or in some case quite down regulated in the *nhp6ab* mutant strain as indicated in Figure 5, pathway 7. Taken together these data confirm that the *nhp6ab* mutant has a reduced glucose utilizing flux along the glycolytic/fermentative pathway.

6. THE DESTINY OF PYRUVATE

Since our data suggest that the *nhp6ab* mutant strain has a reduced glucose glycolytic flux, we wanted to verify (at a transcription level) the fate of pyruvate, derived from the glyceraldehyde 3-P along the second part of the glycolytic way. We then analyzed the level of expression of those genes responsible for the utilization of pyruvate and therefore those forming the cytosolic pyruvate-decarboxylase (*PDC1*, *PDC5* and *PDC6*) through which pyruvate is converted into acetaldehyde (Pathway 8) and those that make up the mitochondrial pyruvate-dehydrogenase complex (*PDA1* and *PDB1*) responsible for the oxidation of pyruvate directly into Acetyl-CoA, inside mitochondria (Pathway 9).

Our data indicate a strong over-expression of *PDA1* and *PDB1* in the *nhp6ab* mutant, suggesting a greater involvement of mitochondria in processing the pyruvate coming from the second part of the glycolysis.

The Acetyl-CoA produced inside the mitochondria on one hand can be exploited to activate the tri-carboxylic acid pathway (TCA) and on the other hand can be converted into acetate. Acetate can freely diffuse into the cytosol where it is again transformed into Acetyl-CoA by Acs1p and Acs2p, increasing the cytosolic pool of this cofactor. In fact, *S. cerevisiae* is devoid of the ATP citrate lyase (Acl) enzyme, responsible in the higher eukaryotes, for shuttling Acetyl-CoA from mitochondria to cytosol. In support of this hypothesis we noticed a significant increase in the expression of the *ACH1* gene for the mutant strain, liable of the conversion of Acetyl-CoA into acetate inside the mitochondria.

The availability of peroxisomal Acetyl-CoA due to the fatty acids beta-oxidation (carried out by *POT1* gene product that is in fact over-expressed in the mutant strain) feeds the glyoxylate cycle, some components of which are found to be over-expressed (Pathway 10). Cells can get energy as well as from glucose degradation, also from triglycerides and

proteins. The former are decomposed into glycerol and fatty acids and enter the Krebs cycle as Acetyl-CoA. The latter are degraded into amino acids whose amino group is transferred to the alpha-ketoglutarate to give glutamate which, in turn, undergoes oxidative deamination leading to ammonium ion and alpha-ketoglutarate which can enter the citric acid cycle. The product of the *GDH2* gene, over-expressed in the mutant strain, is responsible for the reaction.

3.4 Oxidative stress

The transcriptional and metabolic description depicted in the previous section could imply the onset of stress conditions due to the unbalanced redox equilibrium. Therefore we wanted to study the ability of the *nhp6ab* mutant strain to survive to H_2O_2 treatment and compared to that of the WT strain. Evaluation of the results indicate a lower resistance of the mutant cells compared to WT cells (Figure S2A). Moreover the expression of several genes involved in the stress response pathways (divided into categories in Figure S2B) were also considered. In fact as reported by numerous literature data, *S. cerevisiae* cells respond to an increased oxidative stress by up-regulating the expression of several transcription factors [35] and anti-oxidant factors such as catalase and glutathione (36, this work); also the proteasomal degradation of oxidized proteins [37] is part of this oxidative stress response, as well as the autophagic process that undergoes considerable impulse [38].

3.5 Mutation of the *POT1* gene partially restores the global H4 acetylation phenotype in a *nhp6ab* background.

Protein acetylation, hence also that of histone proteins, depends on Acetyl-CoA availability. *nhp6ab* cells show an increased acetylation of the H4K16 residue. Moreover, the metabolic scenario obtained by superimposing transcriptomic and metabolomic data, reported in Figure 5, indicates an increased flux in the production and utilization of this pivotal substance. Hence we focused our attention on the expression of those genes coding for enzymes mostly involved in Acetyl-CoA production: i) *ACS1*, Acetyl-CoA Synthetase isoform 1 [39], which allows the conversion of acetate to Acetyl-CoA, in both cytosol [40] and mitochondrion [41]; ii) *ACS2*, Acetyl-CoA Synthetase isoform 2 [42], which localises in the cytosol [43] and nucleus [44]; iii) *PDA1*, a subunit of the pyruvate dehydrogenase (PDH) complex [45] responsible for the conversion of pyruvate into Acetyl-CoA in the mitochondrion [31]; iv) *POT1*, Peroxisomal Oxoacyl Thiolase [47], which cleaves 3-ketoacyl-CoA into Acyl-CoA and Acetyl-CoA during beta-oxidation of fatty acids [48].

Purified total polyA$^+$ RNA from WT and *nhp6ab* cells was retrotranscribed and amplified by real time PCR using primers for *ACS1*, *ACS2*, *PDA1* and *POT1*. The expression values were normalized to those of *UBC6*. Results (Figure S3) are in agreement with RNA-seq data, and indicate that expression of *ACS1* and *ACS2* is not affected in *nhp6ab* cells, while expression of *PDA1* and *POT1* is significantly increased.

Overall, the expression data support the hypothesis that *nhp6ab* cells might produce more Acetyl-CoA as a consequence of the enhanced *PDA1* and *POT1* expression.

We therefore wanted to evaluate the impact of the fatty acids beta oxidation on histone acetylation, provoking a reduced availability of Acetyl-CoA as a result of its mutation. To this aim we produced, by gene disruption technique, a *pot1* mutant strain and a triple *nhp6ab*/*pot1* mutant. We analyzed their protein extracts by Western Blotting using α-H4K16Ac, α-H4panAc, α-H3panAc or α-H3-Ct (Fig 6). The H4 acetylation level, which is higher in the *nhp6ab* strain (light grey bar) compared to WT (black bar), is reduced in the *nhp6ab*/*pot1* triple mutant (white bar). Notably, the single *pot1* mutation (dark grey bar) does not show any significant difference relative to WT. In addition, acetylation of H3 and H4 revealed by anti-panAc antibodies is clearly decreased in the triple mutant relative to the *nhp6ab* double mutant.

Taken together, these data show that expression of the *POT1* gene is critical in maintaining the increased histone acetylation levels in *nhp6ab* cells, but not in the WT cells.

4. DISCUSSION

Previous studies demonstrated that *nhp6ab* mutant displays an epigenetic perturbation represented by a diminution of histone proteins and a reduced globally distributed nucleosome occupancy. In this work an increased histone acetylation level potentially impacting on gene expression has been showed.

Coherently with the observed reduced nucleosomal occupancy and increased histone acetylation, we measured, by transcriptomic analysis, a substantial alteration in the messenger RNA production in the *nhp6ab* mutant strain. Surprisingly, gene expression change mainly involves metabolic genes. Sensitivity of metabolic genes to chromatin acetylation state is of common knowledge [49]. This makes conceivable to hypothesize that a self sustaining process exists, where histone hyperacetylation, provoking metabolic gene deregulation, leads to an increased supply of Acetyl-CoA. This latter, in turn, allows the hyperacetylated chromatin state to be maintained. To corroborate this hypothesis we reconstructed metabolic pathways of both WT and *nhp6ab* mutant strains and then interrupted one of those that provide Acetyl-CoA, by deleting *POT1* gene. In particular we focused our attention on the metabolic pathways involving glucose and we superimposed transcriptomic and metabolomic data. The evaluation of these –omic approaches allowed us to conclude that glucose utilization along the glycolytic pathway is inefficient. In fact, although glucose uptake into *nhp6ab* cells is higher than in WT, glycolysis appears to be decreased, as suggested by the downregulation of glycolytic genes and the upregulation of non-glycolytic ones (see Figure 5). Indeed, glucose appears to be redirected to the pentose phosphate pathway to produce phosphoribosyl pyrophosphate (PRPP) and nucleotides, in particular uridine mono-, di-

and triphosphate (Figure 5 and table S2). The content of AXP (ATP+ADP) is reduced in *nhp6ab* cells indicative of inefficient ATP synthesis due to reduced glycotic flux. At the same time, the activation of many glyoxylate genes (Figure 5) that bypass the Krebs cycle, suggests reduced synthesis of ATP by the respiratory transport chain, as well.

Overall, the metabolomic analysis suggests that *nhp6ab* cells take up more glucose, but use less of it for energy production, and more for biosynthetic pathways. As a consequence, the cells have a more reductive redox balance, witnessed by the increase in glutathione (table S2).

Moreover the enhanced availability of DHAP feeds a significantly up-regulated metabolic pathway that culminates in the fatty acids production and partially compensates for the redox unbalance arising from the penthose phosphate pathway. The fatty acid beta oxidation carried out by Pot1p, represents a considerable source of Acetyl-CoA. By *POT1* deletion we broke off this step and we were able to partially revert the hyperacetylation phenotype of *nhp6ab*. Thus we demonstrated that the beta oxidation process is necessary to maintain hyperacetylation observed in mutant cells.

Nhp6a and *b* proteins are nor writers, neither erasers or readers of histone modifications. To date they are known only through their architectural functions. This study allowed us to identify, in these two factors, a common element of regulation in metabolism and chromatin acetylation state that could represent a powerful tool to find out relationships existing between metabolism and gene expression in more complex systems.

ACKNOWLEDGEMENTS

This work was supported by the Epigenomics Flagship Project EpiGen, the Italian Ministry of Education and Research, National Research Council; the Istituto Pasteur-Fondazione Cenci Bolognetti, Università di Roma La Sapienza.

REFERENCES

01. Feser, J., Truong, D., Das, C., Carson, J. J., Kieft, J., Harkness, T., & Tyler, J. K. (2010). Elevated Histone Expression Promotes Life Span Extension. Molecular Cell, 39(5), 724–735. https://doi.org/10.1016/j.molcel.2010.08.015

02. O'Sullivan, R. J., Kubicek, S., Schreiber, S. L., & Karlseder, J. (2010). Reduced histone biosynthesis and chromatin changes arising from a damage signal at telomeres. Nature Structural & Molecular Biology, 17(10), 1218–1225. https://doi.org/10.1038/nsmb.1897

03. Eriksson, P. R., Mendiratta, G., McLaughlin, N. B., Wolfsberg, T. G., Marino-Ramirez, L., Pompa, T. A. et al. (2005). Global Regulation by the Yeast Spt10 Protein Is Mediated through Chromatin Structure and the Histone

Upstream Activating Sequence Elements. Molecular and Cellular Biology, 25(20), 9127–9137. https://doi.org/10.1128/MCB.25.20.9127-9137.2005

04. Celona, B., Weiner, A., Di Felice, F., Mancuso, F. M., Cesarini, E., Rossi, R. L., et al. (2011). Substantial histone reduction modulates genomewide nucleosomal occupancy and global transcriptional output. PLoS Biology, 9(6), e1001086. https://doi.org/10.1371/journal.pbio.1001086

05. Stillman, D. J. (2010). Nhp6: A small but powerful effector of chromatin structure in Saccharomyces cerevisiae. Biochimica et Biophysica Acta (BBA) - Gene Regulatory Mechanisms, 1799(1–2), 175–180. https://doi.org/10.1016/j.bbagrm.2009.11.010

06. Kolodrubetz, D., Kruppa, M., & Burgum, A. (2001). Gene dosage affects the expression of the duplicated NHP6 genes of Saccharomyces cerevisiae. Gene, 272(1–2), 93–101.

07. Dowell, N. L., Sperling, A. S., Mason, M. J., & Johnson, R. C. (2010). Chromatin-dependent binding of the S. cerevisiae HMGB protein Nhp6A affects nucleosome dynamics and transcription. Genes & Development, 24(18), 2031–2042. https://doi.org/10.1101/gad.1948910

08. Durano, D., Lukacs, A., Di Felice, F., Micheli, G., & Camilloni, G. (2017). A novel role for Nhp6 proteins in histone gene regulation in Saccharomyces cerevisiae. The International Journal of Biochemistry & Cell Biology, 83, 76–83. https://doi.org/10.1016/j.biocel.2016.12.012

09. Cesarini, E., D'Alfonso, A., & Camilloni, G. (2012). H4K16 acetylation affects recombination and ncRNA transcription at rDNA in Saccharomyces cerevisiae. Molecular Biology of the Cell, 23(14), 2770–2781. https://doi.org/10.1091/mbc.E12-02-0095

10. Janke, R., Dodson, A. E., & Rine, J. (2015). Metabolism and Epigenetics. Annual Review of Cell and Developmental Biology, 31(1) https://doi.org/10.1146/annurev-cellbio-100814-125544

11. Etchegaray, J.-P., & Mostoslavsky, R. (2016). Interplay between Metabolism and Epigenetics: A Nuclear Adaptation to Environmental Changes. Molecular Cell, 62(5), 695–711. https://doi.org/10.1016/j.molcel.2016.05.029

12. Mejia, R. (2011). Not All Genes Are Equal; Shortage of Histones Affects Some Genes More Than Others. PLoS Biology, 9(6), e1001098.

13. Swygert, S. G., & Peterson, C. L. (2014). Chromatin dynamics: Interplay between remodeling enzymes and histone modifications. Biochimica Et Biophysica Acta, 1839(8), 728–736. https://doi.org/10.1016/j.bbagrm.2014.02.013

14. Sherman, F., Fink, G., Hicks, J. (1987) Methods in Yeast Genetics: A Laboratory Course Manual. Cold Spring Harbor Laboratory Press. ISBN 9780879691974

15. Verdone, L., Camilloni, G., Mauro, E. D., & Caserta, M. (1996). Chromatin remodeling during Saccharomyces cerevisiae ADH2 gene activation. Molecular and Cellular Biology, 16(5), 1978–1988.

16. Teste, M.-A., Duquenne, M., François, J. M., & Parrou, J.-L. (2009). Validation of reference genes for quantitative expression analysis by real-time RT-PCR in Saccharomyces cerevisiae. BMC Molecular Biology, 10(1), 99. https://doi.org/10.1186/1471-2199-10-99

17. Langmead, B., Trapnell, C., Pop, M., & Salzberg, S. L. (2009). Ultrafast and memory-efficient alignment of short DNA sequences to the human genome. Genome Biology, 10(3), R25. https://doi.org/10.1186/gb-2009-10-3-r25

18. Li, B., & Dewey, C. N. (2011). RSEM: accurate transcript quantification from RNA-Seq data with or without a reference genome. BMC Bioinformatics, 12, 323. https://doi.org/10.1186/1471-2105-12-323

19. Schurch, N. J., Schofield, P., Gierliński, M., Cole, C., Sherstnev, A., Singh, V., … Barton, G. J. (2016). How many biological replicates are needed in an RNA-seq experiment and which differential expression tool should you use? RNA, 22(6), 839–851. https://doi.org/10.1261/rna.053959.115

20. Love, M. I., Huber, W., & Anders, S. (2014). Moderated estimation of fold change and dispersion for RNA-seq data with DESeq2. Genome Biology, 15(12), 550. https://doi.org/10.1186/s13059-014-0550-8

21. Cherry, J. M. (2015). The Saccharomyces Genome Database: Gene Product Annotation of Function, Process, and Component. Cold Spring Harbor Protocols, 2015(12), pdb.prot088914. https://doi.org/10.1101/pdb.prot088914

22. Edgar, R., Domrachev, M., & Lash, A. E. (2002). Gene Expression Omnibus: NCBI gene expression and hybridization array data repository. Nucleic Acids Research, 30(1), 207–210.

23. Miccheli, A., Ricciolini, R., Piccolella, E., Delfini, M., & Conti, F. (1991). Modulation of human lymphoblastoid B cell line by phorbol ester and sphingosine. A 31P-NMR study. Biochimica Et Biophysica Acta, 1093(1), 29–35.

24. Gorietti, D., Zanni, E., Palleschi, C., Delfini, M., Uccelletti, D., Saliola, M., & Miccheli, A. (2014). Depletion of casein kinase I leads to a NAD(P)+/NAD(P)H balance-dependent metabolic adaptation as determined by NMR spectroscopy-metabolomic profile in Kluyveromyces lactis. Biochimica et Biophysica Acta (BBA) - General Subjects, 1840(1), 556–564. https://doi.org/10.1016/j.bbagen.2013.10.020

25. Miccheli, A., Tomassini, A., Puccetti, C., Valerio, M., Peluso, G., Tuccillo, F. et al. (2006). Metabolic profiling by 13C-NMR spectroscopy: [1,2-13C2]glucose reveals a heterogeneous metabolism in human leukemia T cells. Biochimie, 88(5), 437–448. https://doi.org/10.1016/j.biochi.2005.10.004

26. Zanni, E., Schifano, E., Motta, S., Sciubba, F., Palleschi, C., Mauri, P. et al. (2017). Combination of Metabolomic and Proteomic Analysis Revealed Different Features among Lactobacillus delbrueckii Subspecies bulgaricus and lactis Strains While In Vivo Testing in the Model Organism Caenorhabditis elegans Highlighted Probiotic Properties. Frontiers in Microbiology, 8, 1206. https://doi.org/10.3389/fmicb.2017.01206

27. Fan, T. W.-M., & Lane, A. N. (2016). Applications of NMR spectroscopy to systems biochemistry. Progress in Nuclear Magnetic Resonance Spectroscopy, 92–93, 18–53. https://doi.org/10.1016/j.pnmrs.2016.01.005

28. Wishart, D. S., Jewison, T., Guo, A. C., Wilson, M., Knox, C., Liu, Y. et al. (2013). HMDB 3.0-The Human Metabolome Database in 2013. Nucleic Acids Research, 41(Database issue), D801-807. https://doi.org/10.1093/nar/gks1065

29. Steinhauser, S., Kurzawa, N., Eils, R., & Herrmann, C. (2016). A comprehensive comparison of tools for differential ChIP-seq analysis. Briefings in Bioinformatics, 17(6), 953–966. https://doi.org/10.1093/bib/bbv110

30. Shia, W.-J., Li, B., & Workman, J. L. (2006). SAS-mediated acetylation of histone H4 Lys 16 is required for H2A.Z incorporation at subtelomeric regions in Saccharomyces cerevisiae. Genes & Development, 20(18), 2507–2512. https://doi.org/10.1101/gad.1439206

31. Oppikofer, M., Kueng, S., Martino, F., Soeroes, S., Hancock, S. M., Chin, J. W. et al. M. (2011). A dual role of H4K16 acetylation in the establishment of yeast silent chromatin: Dual role of H4K16 ac in yeast silencing. The EMBO Journal, 30(13), 2610–2621. https://doi.org/10.1038/emboj.2011.170

32. Saliola, M., Tramonti, A., Lanini, C., Cialfi, S., Biase, D. D., & Falcone, C. (2012). Intracellular NADPH Levels Affect the Oligomeric State of the Glucose 6-Phosphate Dehydrogenase. Eukaryotic Cell 11, 1503–1511. https://doi.org/10.1128/EC.00211-12

33. Boles, E., Lehnert, W., & Zimmermann, F. K. (1993). The role of the NAD-dependent glutamate dehydrogenase in restoring growth on glucose of a Saccharomyces cerevisiae phosphoglucose isomerase mutant. European Journal of Biochemistry, 217(1), 469–477.

34. Pronk, J. T., Steensma, H. Y., & Dijken, J. P. V. (1996). Pyruvate Metabolism in Saccharomyces cerevisiae. Yeast, 12(16), 1607–1633. https://doi.org/10.1002/(SICI)1097-0061(199612)12:16<1607::AID-YEA70>3.0.CO;2-4

35. Hong, S.-Y., Roze, L. V., & Linz, J. E. (2013). Oxidative Stress-Related Transcription Factors in the Regulation of Secondary Metabolism. Toxins, 5(4), 683–702. https://doi.org/10.3390/toxins5040683

36. Fernandes, P. N., Mannarino, S. C., Silva, C. G., Pereira, M. D., Panek, A. D., & Eleutherio, E. C. A. (2007). Oxidative stress response in eukaryotes: effect of glutathione, superoxide dismutase and catalase on adaptation to peroxide and menadione stresses in Saccharomyces cerevisiae. Redox Report, 12(5), 236–244. https://doi.org/10.1179/135100007X200344

37. Höhn, T. J. A., & Grune, T. (2014). The proteasome and the degradation of oxidized proteins: part III-Redox regulation of the proteasomal system. Redox Biology, 2, 388–394. https://doi.org/10.1016/j.redox.2013.12.029

38. Farrugia, G., & Balzan, R. (2012). Oxidative stress and programmed cell death in yeast. Frontiers in Oncology, 2, 64. https://doi.org/10.3389/fonc.2012.00064

39. De Virgilio, C., Bürckert, N., Barth, G., Neuhaus, J. M., Boller, T., & Wiemken, A. (1992). Cloning and disruption of a gene required for growth on acetate but not on ethanol: the acetyl-coenzyme A synthetase gene of Saccharomyces cerevisiae. Yeast (Chichester, England), 8(12), 1043–1051. https://doi.org/10.1002/yea.320081207

40. de Jong-Gubbels, P., van den Berg, M. A., Luttik, M. A., Steensma, H. Y., van Dijken, J. P., & Pronk, J. T. (1998). Overproduction of acetyl-coenzyme A synthetase isoenzymes in respiring Saccharomyces cerevisiae cells does not reduce acetate production after exposure to glucose excess. FEMS Microbiology Letters, 165(1), 15–20.

41. Reinders, J., Zahedi, R. P., Pfanner, N., Meisinger, C., & Sickmann, A. (2006). Toward the complete yeast mitochondrial proteome: multidimensional separation techniques for mitochondrial proteomics. Journal of Proteome Research, 5(7), 1543–1554. https://doi.org/10.1021/pr050477f

42. Van den Berg, M. A., & Steensma, H. Y. (1995). ACS2, a Saccharomyces cerevisiae gene encoding acetyl-coenzyme A synthetase, essential for growth on glucose. European Journal of Biochemistry, 231(3), 704–713.

43. Takahashi, H., McCaffery, J. M., Irizarry, R. A., & Boeke, J. D. (2006). Nucleocytosolic Acetyl-Coenzyme A Synthetase Is Required for Histone Acetylation and Global Transcription. Molecular Cell, 23(2), 207–217. https://doi.org/10.1016/j.molcel.2006.05.040

44. Falcón, A. A., Chen, S., Wood, M. S., & Aris, J. P. (2010). Acetyl-coenzyme A synthetase 2 is a nuclear protein required for replicative longevity in Saccharomyces cerevisiae. Molecular and Cellular Biochemistry, 333(1–2), 99–108. https://doi.org/10.1007/s11010-009-0209-z

45. Steensma, H. Y., Holterman, L., Dekker, I., van Sluis, C. A., & Wenzel, T. J. (1990). Molecular cloning of the gene for the E1 alpha subunit of the pyruvate dehydrogenase complex from Saccharomyces cerevisiae. European Journal of Biochemistry, 191(3), 769–774.

46. Sickmann, A., Reinders, J., Wagner, Y., Joppich, C., Zahedi, R., Meyer, H. E. et al. (2003). The proteome of Saccharomyces cerevisiae mitochondria. Proceedings of the National Academy of Sciences of the United States of America, 100(23), 13207–13212. https://doi.org/10.1073/pnas.2135385100

47. Igual, J. C., Matallaná, E., Gonzalez-Bosch, C., Franco, L., & Pérez-Ortin, J. E. (1991). A new glucose-repressible gene identified from the analysis of chromatin structure in deletion mutants of yeast SUC2 locus. Yeast (Chichester, England), 7(4), 379–389. https://doi.org/10.1002/yea.320070408

48. Mathieu, M., Modis, Y., Zeelen, J. P., Engel, C. K., Abagyan, R. A., Ahlberg, A. et al. (1997). The 1.8 A crystal structure of the dimeric peroxisomal 3-ketoacyl-CoA thiolase of Saccharomyces cerevisiae: implications for substrate binding and reaction mechanism. Journal of Molecular Biology, 273(3), 714–728. https://doi.org/10.1006/jmbi.1997.1331

49. Guan, K.-L., & Xiong, Y. (2011). Regulation of intermediary metabolism by protein acetylation. Trends in Biochemical Sciences, 36(2), 108–116. https://doi.org/10.1016/j.tibs.2010.09.003

Legends to the figures

Fig.1 H4K16 hyperacetylation in *nhp6ab* strain. Western blot analysis of whole cells extracts from WT and *nhp6ab* analyzed for histone H4K16 Acetylation. H3Ct was used as loading control. WT H4K16Ac/H3 ratio is given as 1.

Fig.2 H4K16Ac distribution along chromosomes IV, XII and XIII (as samples of all chromosomes). ChIP-seq data are reported as *nhp6ab*/WT log ratio. Positive peaks indicate H4K16Ac enrichment in *nhp6ab* mutant; negative peaks indicate H4K16Ac enrichment in WT.

Fig.3 Superimposition of RNA-seq, ChIP-seq and MNase-seq data. A: Relationships between differential H4K16Ac enrichments and nucleosome occupancy in WT and *nhp6ab*. H4K16Ac enrichments (ChIP-seq data) have been matched with nucleosome occupancy (MNase-seq data) thus providing informations on nucleosome acetylation. "Specific" or "common" nucleosomes refer to nucleosome positions (MNase-seq mapped) where overlapping between WT and *nhp6ab* is <75% or > 75% respectively. "All" refers to any position occupied by a nucleosome (MNase-seq mapped). RMKN (Reads per Million per Kilobase per Nucleosome). B: Distribution of transcripts levels (two biological replicates) in WT and *nhp6ab*, obtained by RNA-seq analysis. C: Relationship among H4K16Ac, nucleosome occupancy and transcription. All nucleosome acetylation data, obtained as in A (all nucs) have been matched with transcription data of all regions containing genes (genes), upregulated (up) or downregulated (down). Each comparison between WT and mutant box plots gives a significant (*) p-value ($<2.2 \cdot 10^{-16}$). The statistical test employed is Mann–Whitney U test.

Fig.4 Metabolome analysis. Medium metabolite changes expressed as net balance of concentration between cell and medium. Aqueous extract phases from WT and *nhp6ab* cells growing on glucose and their culture media, were subjected to NMR analysis. The culture medium was used to calculate the external metabolite balances (before and after growth). Metabolite flux is indicated by positive signs (from cell to medium) or negative signs (from medium to cell)

Fig.5 Selected pathways of glucose metabolism and succeeding transformations in *nhp6ab* strain as deduced by RNA-seq, metabolomic and biochemical analyses. Main pathways are numbered (1-10) and boxed in color (red for efficiently

used, blue for inefficiently used). Mitochondrial pathways (9) are dot boxed. Up-regulated genes coding for the enzymes responsible for specific transformations are reported in red.

Fig.6 Western blot analysis of whole cells extracts from WT, *nhp6ab*, *pot1* and *nhp6ab*/*pot1* for H3 and H4 acetylation. Histone H4 acetylation of the specific K16 residue (H4K16Ac) and at residues K5, 8, 12 and 16 were measured by anti-acetyl H4K16 and H4-PanAc antibodies respectively. Histone H3 acetylation has been measured by anti H3 acetyl antibodies against N-terminus acetylated residues. H3Ct was used as loading control. Quantifications of western analyses is reported (bottom).

Table 1

Gene Ontology - Biological process

Up regulated genes > 1.5	
Category	**p-value**
glycerol transport [GO:0015793]	0,000355482
carbohydrate transport [GO:0008643]	0,000374024
ammonia assimilation cycle [GO:0019676]	0,000858879
maltose metabolic process [GO:0000023]	0,00105597
regulation of transcription involved in G1 phase of mitotic cell cycle [GO:0000114]	0,00166023
regulation of glycolysis by positive regulation of transcription from an RNA polymerase II promoter [GO:0072363]	0,00204395
transmembrane transport [GO:0055085]	0,00249812
proline catabolic process [GO:0006562]	0,00594793
positive regulation of translation in response to stress [GO:0032056]	0,00594793
meiotic sister chromatid cohesion [GO:0051177]	0,00594793
gamma-aminobutyric acid transport [GO:0015812]	0,00594793
re-entry into mitotic cell cycle after pheromone arrest [GO:0000321]	0,00629861
nucleosome assembly [GO:0006334]	0,00761761

Down regulated genes > 1.5	
Category	**p-value**
translation [GO:0006412]	1,00E-014
metabolic process [GO:0008152]	3,73E-013
oxidation-reduction process [GO:0055114]	7,97E-013
cellular amino acid biosynthetic process [GO:0008652]	2,33E-012
phospholipid biosynthetic process [GO:0008654]	5,81E-008
ribosomal large subunit assembly [GO:0000027]	3,56E-006
ribosome biogenesis [GO:0042254]	2,05E-005
regulation of translational fidelity [GO:0006450]	2,96E-005
arginine biosynthetic process [GO:0006526]	2,96E-005
rRNA export from nucleus [GO:0006407]	3,33E-005
methylation [GO:0032259]	6,75E-005
maturation of SSU-rRNA from tricistronic rRNA transcript (SSU-rRNA, 5.8S rRNA, LSU-rRNA) [GO:0000462]	7,67E-005
cellular amino acid metabolic process [GO:0006520]	9,03E-005
fatty acid biosynthetic process [GO:0006633]	0,00014332
translational elongation [GO:0006414]	0,00014332
tRNA aminoacylation for protein translation [GO:0006418]	0,00019679
cellular response to oxidative stress [GO:0034599]	0,00032445
ribosomal small subunit assembly [GO:0000028]	0,00034256
lysine biosynthetic process [GO:0009085]	0,00038322
aromatic amino acid family biosynthetic process [GO:0009073]	0,00039287
endonucleolytic cleavage in ITS1 to separate SSU-rRNA from 5.8S rRNA and LSU-rRNA from tricistronic rRNA transcript (SSU-rRNA, 5.8S rRNA, LSU-rRNA) [GO:0000447]	0,00056578
apoptosis [GO:0006915]	0,00069992
de novo NAD biosynthetic process from tryptophan [GO:0034354]	0,00098175
response to toxin [GO:0009636]	0,00098175
glycolysis [GO:0006096]	0,00111569
sulfate assimilation [GO:0000103]	0,00119343
methionine biosynthetic process [GO:0009086]	0,00129704
phosphatidylcholine biosynthetic process [GO:0006656]	0,00134934
tryptophan catabolic process [GO:0006569]	0,00134978
iron ion homeostasis [GO:0055072]	0,00152823
rRNA processing [GO:0006364]	0,00327387
proteasome regulatory particle assembly [GO:0070682]	0,00352376
response to oxidative stress [GO:0006979]	0,00352376
phosphatidylethanolamine biosynthetic process [GO:0006646]	0,0039264
folic acid biosynthetic process [GO:0046656]	0,0039264
aromatic amino acid family catabolic process to alcohol via Ehrlich pathway [GO:0000949]	0,0039264
endonucleolytic cleavage to generate mature 3'-end of SSU-rRNA from (SSU-rRNA, 5.8S rRNA, LSU-rRNA) [GO:0000461]	0,0039264
carboxylic acid metabolic process [GO:0019752]	0,00424944
siderophore transport [GO:0015891]	0,00424944
lysine biosynthetic process via aminoadipic acid [GO:0019878]	0,00424944
lipid biosynthetic process [GO:0008610]	0,00465854
deoxyribonucleotide biosynthetic process [GO:0009263]	0,00466368
gluconeogenesis [GO:0006094]	0,00544393
ribosomal subunit export from nucleus [GO:0000054]	0,00567761
glutamine metabolic process [GO:0006541]	0,00644636
chronological cell aging [GO:0001300]	0,0075055
ion transport [GO:0006811]	0,00975191

Figure 1

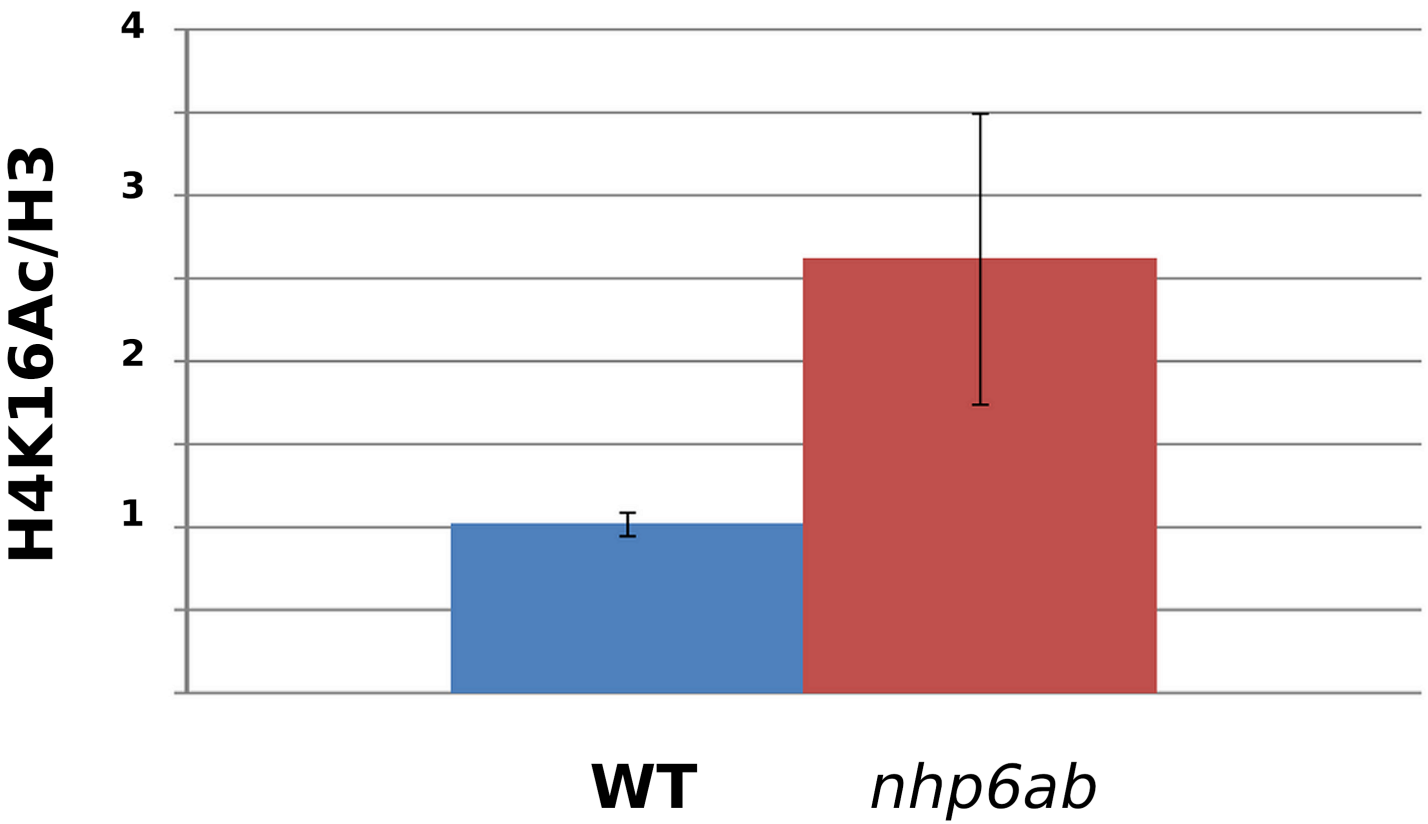

Figure 2

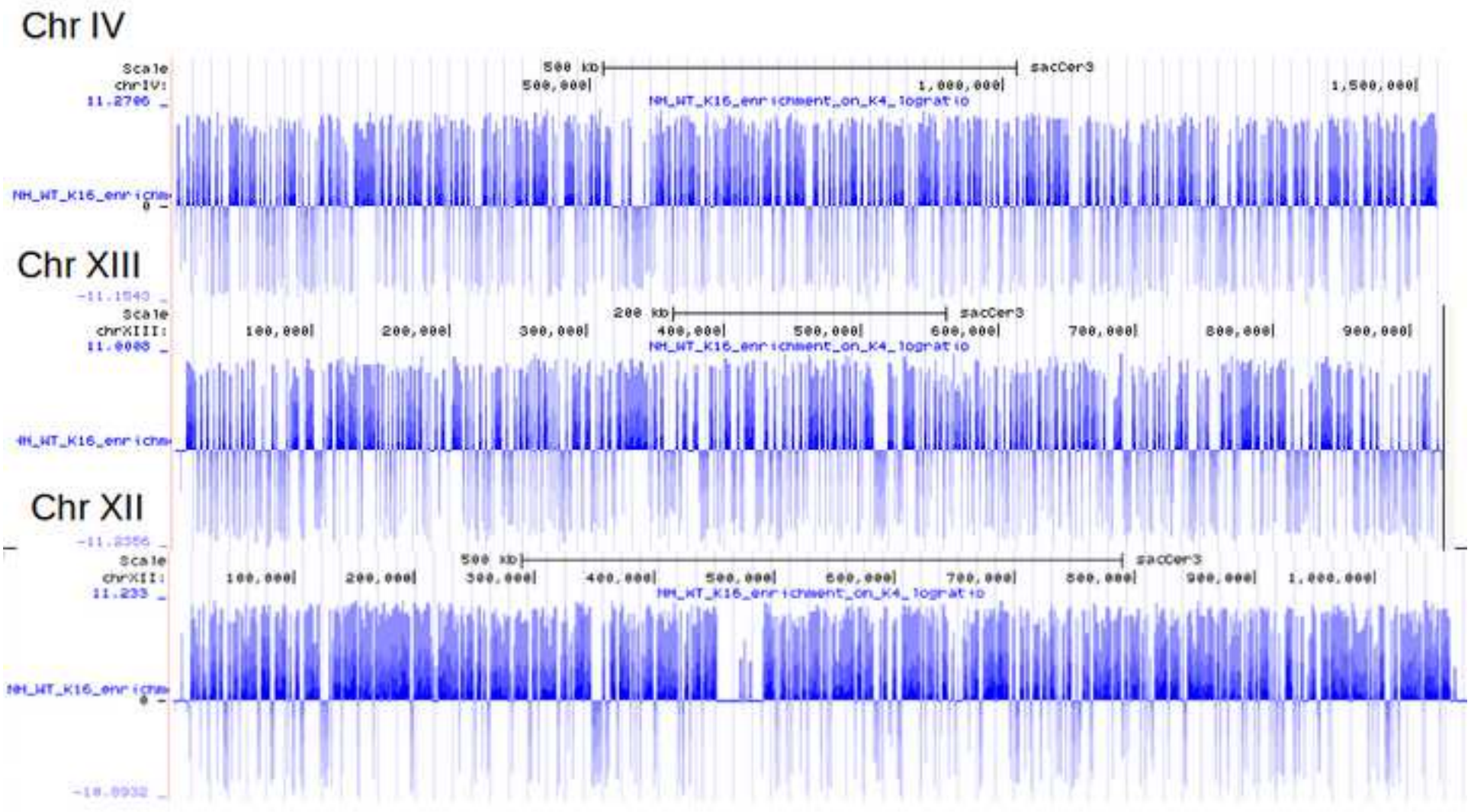
Chr IV
Scale
chrIV:
11,2700
500 kb
500,000
1,000,000
sacCer3
1,500,000
NH_WT_K16_enrichment_on_K4_logratio
NH_WT_K16_enrichme
0
Chr XIII
-11,1540
Scale
chrXIII:
11,0000
200 kb
sacCer3
100,000
200,000
300,000
400,000
500,000
600,000
700,000
800,000
900,000
NH_WT_K16_enrichment_on_K4_logratio
NH_WT_K16_enrichme
Chr XII
-11,2356
Scale
chrXII:
11,233
500 kb
sacCer3
100,000
200,000
300,000
400,000
500,000
600,000
700,000
800,000
900,000
1,000,000
NH_WT_K16_enrichment_on_K4_logratio
NH_WT_K16_enrichme
0
-10,0932

Figure 3

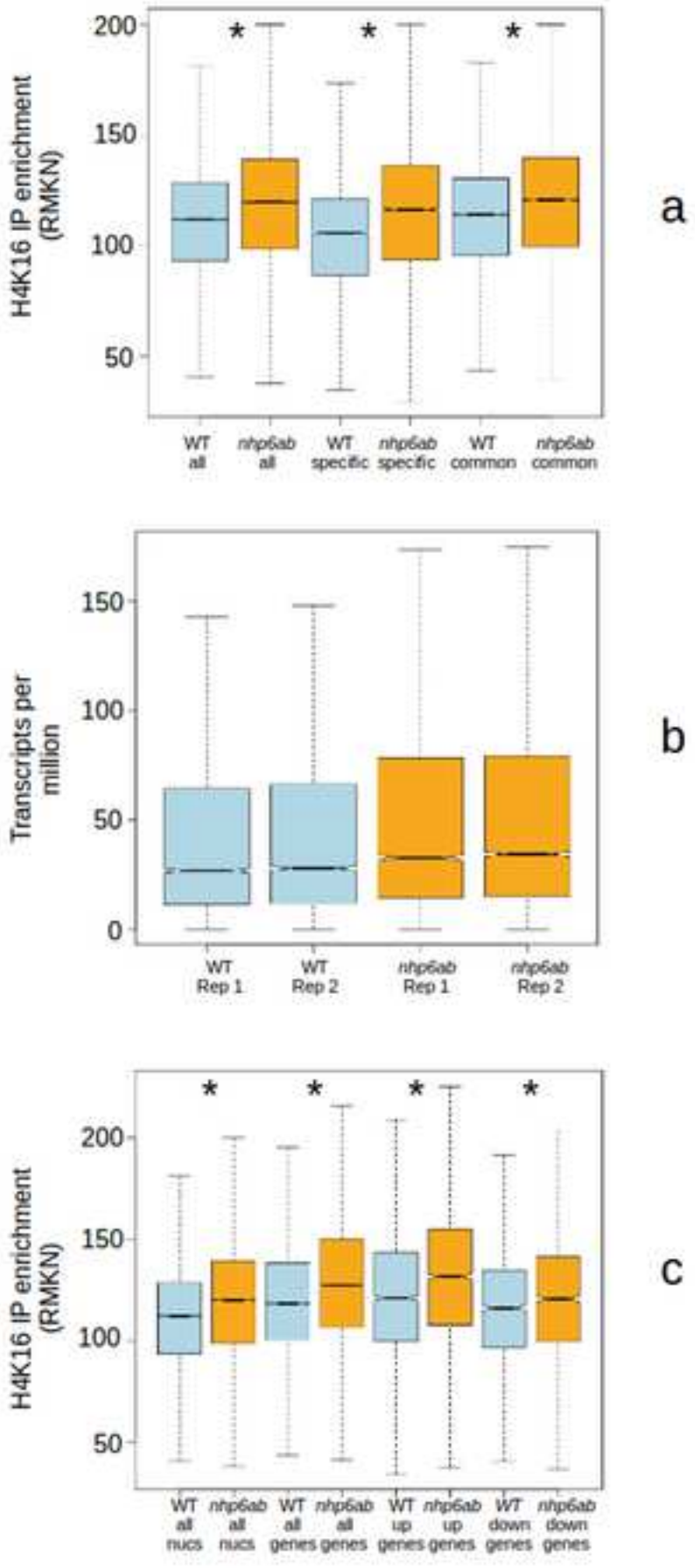
H4K16 IP enrichment (RMKN)
200
150
100
50
*
*
*
WT all
nhp6ab all
WT specific
nhp6ab specific
WT common
nhp6ab common
a
Transcripts per million
150
100
50
0
WT Rep 1
WT Rep 2
nhp6ab Rep 1
nhp6ab Rep 2
b
H4K16 IP enrichment (RMKN)
200
150
100
50
*
*
*
*
WT all nucs
nhp6ab all nucs
WT all genes
nhp6ab all genes
WT up genes
nhp6ab up genes
WT down genes
nhp6ab down genes
c

Figure 4

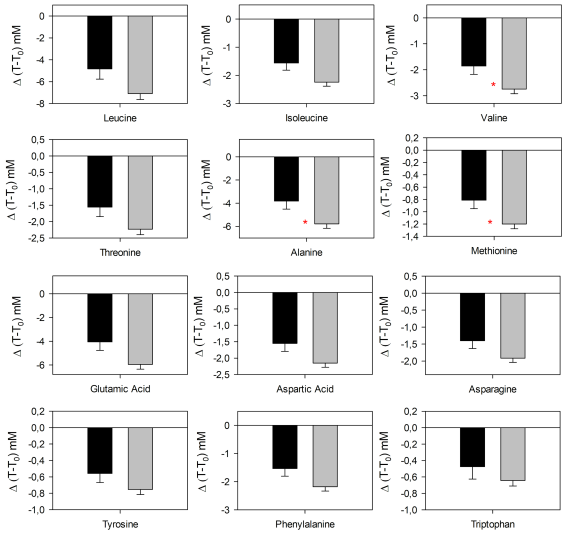
Aminoacids
Δ (T-T0) mM
Leucine
Isoleucine
Valine
Threonine
Alanine
Methionine
Glutamic Acid
Aspartic Acid
Asparagine
Tyrosine
Phenylalanine
Triptophan

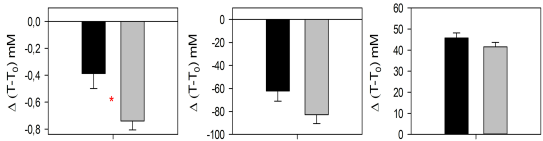
Carbohydrates and miscellaneous
Δ (T-T0) mM
Trehalose
Glucose
Raffinose

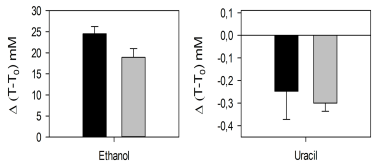
Δ (T-T0) mM
Ethanol
Uracil

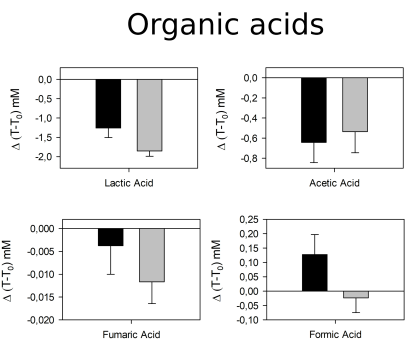
Organic acids
Δ (T-T0) mM
Lactic Acid
Acetic Acid
Fumaric Acid
Formic Acid

Figure 5

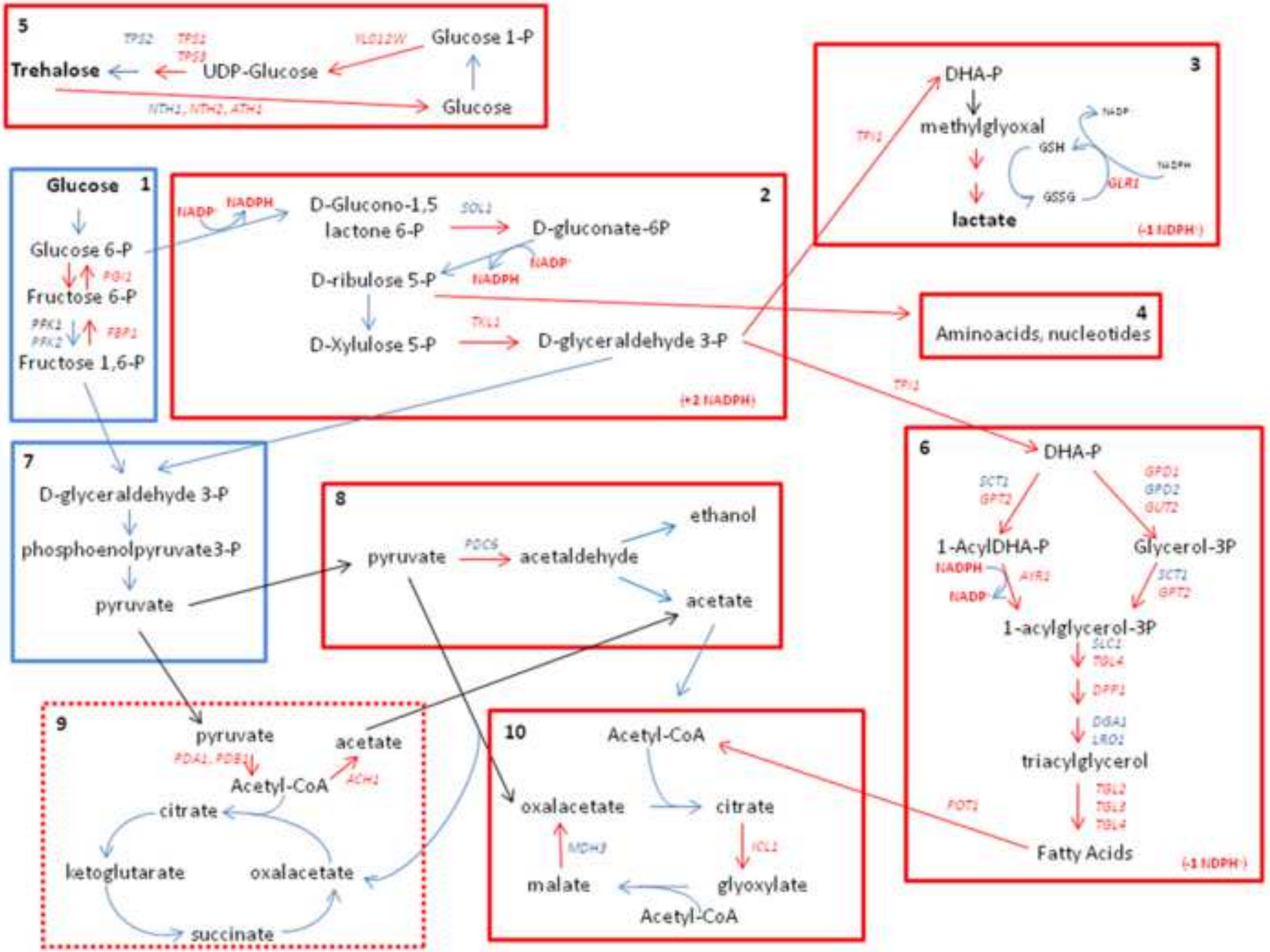
5
TPS2
TPS1
TPS3
YLR12W
Glucose 1-P
Trehalose
UDP-Glucose
NTH1, NTH2, ATH1
Glucose
Glucose 1
Glucose 6-P
PGI1
Fructose 6-P
PFK1
PFK2
FBP1
Fructose 1,6-P
2
NADP
NADPH
D-Glucono-1,5 lactone 6-P
SOL3
D-gluconate-6P
NADP
D-ribulose 5-P
NADPH
D-Xylulose 5-P
TKL1
D-glyceraldehyde 3-P
(+2 NADPH)
3
DHA-P
methylglyoxal
TPI1
NADP
GSH
NADPH
GSSG
GLR1
lactate
(-1 NADPH)
4
Aminoacids, nucleotides
TPI1
6
DHA-P
SCT1
GPT2
GPD1
GPD2
GUT2
1-AcylDHA-P
Glycerol-3P
NADPH
NADP
AYR1
SCT1
GPT2
1-acylglycerol-3P
SLC1
TGL4
DPP1
DGA1
LRO1
triacylglycerol
TGL3
TGL5
TGL4
FOT1
Fatty Acids
(-1 NADPH)
7
D-glyceraldehyde 3-P
phosphoenolpyruvate3-P
pyruvate
8
pyruvate
PDC5
acetaldehyde
ethanol
acetate
9
pyruvate
acetate
PDA1, PDB1
ACH1
Acetyl-CoA
citrate
ketoglutarate
oxalacetate
succinate
10
Acetyl-CoA
oxalacetate
citrate
MDH3
ICL1
malate
glyoxylate
Acetyl-CoA

Figure 6

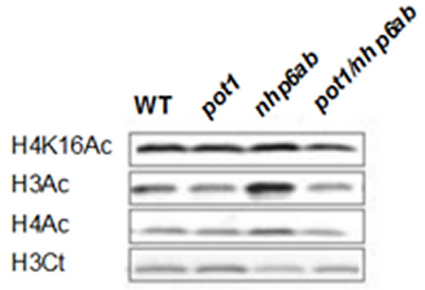
WT
pot1
nhp6ab
pot1/nhp6ab
H4K16Ac
H3Ac
H4Ac
H3Ct

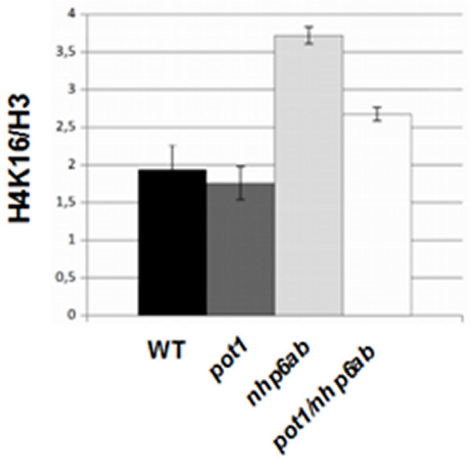
H4K16/H3
WT
pot1
nhp6ab
pot1/nhp6ab

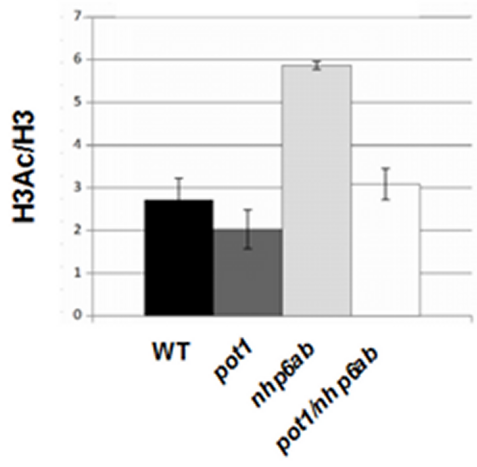
H3Ac/H3
WT
pot1
nhp6ab
pot1/nhp6ab

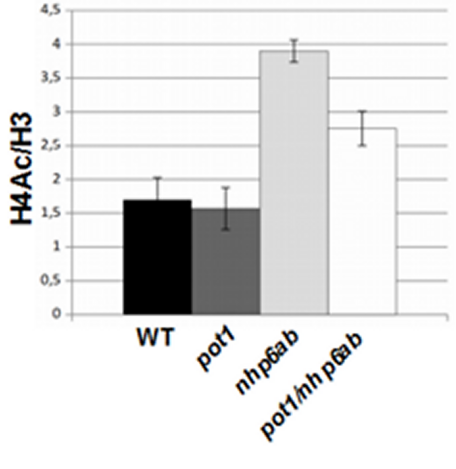
H4Ac/H3
WT
pot1
nhp6ab
pot1/nhp6ab

Table S1

Click here to download Supplementary Material (for online publication): S1 tab.pdf

S1 Table. Resonance assignement.

Compound	Assignment[a]	^{1}H (ppm)	Multiplicity[b]	Location[c]
Amino acids				
Valine (Val)	α -CH β-CH **γ-CH_3** γ'-CH_3	3,62 2,29 **1,05** 1,00	m m **d** d	C, E
Isoleucine (Ile)	α -CH β-CH γ-CH γ'-CH **δ-CH_3** δ'-CH_3	3,69 1,99 1,25 1,49 **1,01** 0,95	m m m m **d** t	C, E
Leucine (Leu)	α -CH β-CH_2 γ-CH_3 **δ -CH_3** **δ'-CH_3**	3,74 1,73 1,69 **0,97** **0,96**	m m m **d** **d**	C, E
Alanine (Ala)	α-CH **β-CH_3**	3,77 **1,49**	q **d**	C, E
Methionine (Met)	α -CH β-CH_2 γ-CH_3 **S -CH_3**	3,85 2,18 2,64 **2,14**	m m m **s**	E
Threonine (Thr)	α-CH β-CH **γ-CH_3**	3,57 4,24 **1,33**	d m **d**	C, E
Glutamic acid (Glu)	α-CH β-CH_2 **γ-CH_2**	3,74 2,08 **2,36**	t dt **t**	C, E
Glutamine (Gln)	α-CH β-CH_2 **γ-CH_2**	3,76 2,11 **2,45**	t dt **t**	C
Glutathione (GSH)	α-CH Glu β-CH_2 Glu **γ-CH_2 Glu** α-CH Cysteine β-CH_2 Cysteine α-CH_2 Gly	3,78 2,17 **2,56** 4,19 3,78 3,76	t dt **t** m m s	C
Aspartic acid (Asp)	α-CH **β-CH** β'-CH	3,90 **2,63** 2,70	dd **dd** dd	C, E
Asparagine (Asn)	α-CH β-CH **β'-CH**	3,99 2,71 **2,82**	dd dd **dd**	C, E
Lysine (Lys)	α-CH β-CH_2	3,74 1,89	m m	C

	γ-CH_2 δ-CH_2 **ε-CH_2**	1,71 1,43 3,03	m m **t**	
Arginine (Arg)	α-CH β-CH_2 γ-CH_2 **δ-CH_2**	3,76 1,92 1,69 **3,25**	m m m **t**	C
Glycine (Gly)	**α-CH_2**	**3,69**	**s**	C
Tyrosine (Tyr)	α-CH β-CH β'-CH C2,6H-ring **C3,5H-ring**	3,93 3,15 3,05 7,20 **6,90**	dd dd dd d **d**	C, E
Phenylalanine (Phe)	C2,6H-ring CH-4 ring **C3,5H-ring**	7,33 7,39 **7,42**	m m **m**	C, E
Histidine (His)	**C2H ring** C5H ring	**7.13** 8.02	**s** s	C
Triptophan (Trp)	CH-5 ring CH-6 ring CH-7 ring **CH-4 ring**	7,20 7,27 7,54 **7,74**	t t d **d**	E
Organic Acids				
Acetic acid (AA)	**CH_3**	**1,93**	**s**	C, E
Fumaric acid (Fuma)	**α,β-CH=CH**	**6,51**	**s**	C, E
Succinic acid (SA)	**α,β-CH_2**	**2,41**	**s**	C
Lactic acid (LA)	α-CH **β-CH**	4,12 **1,37**	q **d**	C, E
Formic acid (FA)	**CH**	**8,46**	**s**	C, E
Carbohydrates				
α-Glucose (α-G)	**CH-1** CH-2 CH-3 CH-4 CH-5 CH_2-6	**5,23** 3,55 3,72 3,42 3,84 3,73 – 3,90	**d** m m m m m	C, E
β-Glucose (β-G)	CH-1 **CH-2** CH-3 CH-4 CH-5 CH_2-6	4,65 **3,24** 3,50 3,42 3,48 3,74 – 3,91	d **dd** m m m m	C, E
Trehalose (T)	**CH-1,1'**	**5,19**	**d**	C, E

	CH-2,2' CH-3,3' CH-4,4' CH-5,5' CH_2-6,6'	3,64 3,76 3,44 3,82 3,79 – 3,88	m m m m m	
Raffinose (R)	CH-1 G **CH-1 Galactose** CH-3 F	5,44 **5,01** 4,22	d **d** d	E
Miscellaneous Compounds				
Ethanol (Eth)	CH_2 **CH_3**	3,66 1,19	q **t**	E
1,2-propanediol (PDP)	α-CH_2 β-CH **γ-CH_3**	3,43 – 3,53 3,89 **1,15**	m m **d**	C
U1	**-CH_3**	**2,97**	**s**	C
Uracil (Ura)	**C5H** C6H	**5,80** 7,74	**d** d	E
Uridine Monophosphate (UMP)	**C5H ring Ura** C6H ring Ura	**5,90** 7,89	**d** d	C
Uridine Diphosphate (UDP)	**C5H ring Ura** C6H ring Ura	**5,97** 7,95	**d** d	C
Uridine Triphosphate (UTP)	**C5H ring Ura** C6H ring Ura	**5,99** 7,98	**d** d	C
Cytosine Diphosphate (CDP)	**C5H ring Cyt** C6H ring Cyt	**6,14** 7,98	**d** d	C
Cytosine Triphosphate (CTP)	**C5H ring Cyt** C6H ring Cyt	**6,15** 7,99	**d** d	C
Guanosine Phosphate (GXP)	**C8H ring Gua** **C8H ring Gua**	**8,15** **8,21**	**s** **s**	C
Adenosine Phosphate (AXP)	C2H ring Ade **C8H ring Ade**	8,23 **8,58**	s **s**	C
NAD	**C2H Nam** C4H Nam C5H Nam C6H Nam	**9,34** 8,84 8,29 9,15	**s** m m m	C
Nicotinamide riboside (NamRib)	**C2H Nam** C4H Nam C5H Nam C6H Nam	**9,61** 8,89 8,31 9,34	**s** m m m	C

[a] specific resonance signal used for quantization are reported in bold.

[b] s: singlet; d: doublet; dd: double doublet; dt: double triplet; t: triplet; q: quartet; m: multiplet

[c] C: cytosol; E: extracellular

Table S2

Click here to download Supplementary Material (for online publication): S2 tab.pdf

S2 Table. Metabolite concentrations.

	WT (n = 6)	nhp6ab (n = 8)	
Leucine	1.89 ± 0.17	2.60 ± 0.12	0.009546
Isoleucine	0.89 ± 0.05	1.34 ± 0.08	0.000213
Valine	1.41 ± 0.08	1.84 ± 0.12	0.008871
Threonine	0.94 ± 0.05	2.08 ± 0.25	0.000251
Alanine	4.29 ± 0.17	7.87 ± 0.85	0.000469
Glutamate	13.61± 0.61	16.17 ± 1.24	n.s
Glutamine	1.09 ± 0.10	1.54 ± 0.05	0.003018
Glutathione	1.73 ± 0.08	2.36 ± 0.21	0.008347
Aspartate	1.30 ± 0.07	1.55 ± 0.07	0.038665
Asparagine	4.68 ± 0.27	5.96 ± 0.20	0.003897
Lysine	4.35 ± 0.27	4.84 ± 0.25	n.s
Arginine	5.08 ± 0.33	7.37 ± 0.38	0.00064
Glycine	2.14 ± 0.09	1.67 ± 0.15	0.014034
Tyrosine	0.35 ± 0.02	0.52 ± 0.03	0.000428
Histidine	2.80 ± 0.18	1.27 ± 0.60	0.017635
Phenylalanine	0.55 ± 0.04	1.05 ± 0.07	2.68E-05
Lactate	0.21 ± 0.01	0.47 ± 0.06	0.000221
Acetate	8.11 ± 0.57	8.60 ± 0.21	n.s
Succinate	0.23 ± 0.01	0.21 ± 0.02	n.s
Fumarate	0.04 ± 0.01	0.03 ± 0.00	n.s.
Formate	0.13 ± 0.01	0.13 ± 0.01	n.s.
Trealose	0.04 ± 0.00	0.10 ± 0.01	8.28E-07
Glucose	0.33 ± 0.02	0.61 ± 0.07	0.000902
1,2 propandiol	1.44 ± 0.03	1.58 ± 0.03	0.004822
U1	0.48 ± 0.02	0.56 ± 0.02	0.036819
UTP	0.17 ± 0.01	0.25 ± 0.01	0.000174
UDP	0.11 ± 0.01	0.29 ± 0.02	2.12E-06
UMP	0.39 ± 0.03	0.63 ± 0.03	6.37E-05
CTP	0.21 ± 0.02	0.28 ± 0.03	n.s
CMP	0.50 ± 0.03	0.41 ± 0.03	n.s
GTP + GDP (GXP)	0.38 ± 0.04	0.37 ± 0.02	n.s
ATP + ADP (AXP)	0.37 ± 0.04	0.13 ± 0.05	0.002641
NAD	0.48 ± 0.03	0.43 ± 0.03	0.255313
Nam-Ribose	0.04 ± 0.01	0.01 ± 0.01	0.00509

Table …: Intracellular metabolite concentrations expressed as means and Standard Deviation (SD) of μmol/g biomass weight. Unpaired data Student's t test was used to compare the differences.

Tab S3

Click here to download Supplementary Material (for online publication): S3_tab.pdf

Down regulated genes >1.5

GO Molecular Function

Category	p-value	k	f
structural constituent of ribosome [GO:0003735]	1,00E-014	79	218
lyase activity [GO:0016829]	2,35E-008	23	79
oxidoreductase activity [GO:0016491]	2,22E-007	47	272
catalytic activity [GO:0003824]	7,24E-007	66	455
carboxy-lyase activity [GO:0016831]	3,28E-005	8	18
rRNA binding [GO:0019843]	0,000157771	11	39
pyridoxal phosphate binding [GO:0030170]	0,000404035	11	43
transferase activity, transferring acyl groups, acyl groups converted into alkyl on transfer [GO:0046912]	0,00114694	4	7
NAD binding [GO:0051287]	0,00155149	7	23
magnesium ion binding [GO:0000287]	0,00186714	11	51
amino acid binding [GO:0016597]	0,00189191	3	4
SSU rRNA binding [GO:0070181]	0,00189191	3	4
pyruvate decarboxylase activity [GO:0004737]	0,00189191	3	4
peptidase inhibitor activity [GO:0030414]	0,00189191	3	4
thiamine pyrophosphate binding [GO:0030976]	0,0021499	4	8
hexokinase activity [GO:0004396]	0,00444982	3	5
homocitrate synthase activity [GO:0004410]	0,00633473	2	2
acetolactate synthase activity [GO:0003984]	0,00633473	2	2
tricarboxylate secondary active transmembrane transporter activity [GO:0005371]	0,00633473	2	2
arylformamidase activity [GO:0004061]	0,00633473	2	2
methionine adenosyltransferase activity [GO:0004478]	0,00633473	2	2
oxidoreductase activity, acting on a sulfur group of donors, disulfide as acceptor [GO:0016671]	0,00633473	2	2
3-hydroxyacyl-[acyl-carrier-protein] dehydratase activity [GO:0019171]	0,00633473	2	2
fatty-acyl-CoA synthase activity [GO:0004321]	0,00633473	2	2
2-isopropylmalate synthase activity [GO:0003852]	0,00633473	2	2
serine-type endopeptidase inhibitor activity [GO:0004867]	0,00633473	2	2
CTP synthase activity [GO:0003883]	0,00633473	2	2
alcohol O-acetyltransferase activity [GO:0004026]	0,00837508	3	6

GO Cellular Component

Category	p-value	k	f
cytosolic small ribosomal subunit [GO:0022627]	1,00E-014	37	62
cytosolic large ribosomal subunit [GO:0022625]	1,00E-014	42	88
ribonucleoprotein complex [GO:0030529]	1,00E-014	81	307
ribosome [GO:0005840]	1,00E-014	81	310
intracellular [GO:0005622]	1,00E-014	76	381
cytoplasm [GO:0005737]	2,14E-009	223	2026
small ribosomal subunit [GO:0015935]	4,09E-005	7	14
extracellular region [GO:0005576]	4,39E-005	20	95
fungal-type cell wall [GO:0009277]	9,70E-005	18	85
cell wall [GO:0005618]	0,000768997	14	68
cytosol [GO:0005829]	0,0011918	28	192
vacuolar transporter chaperone complex [GO:0033254]	0,00189191	3	4
anchored to membrane [GO:0031225]	0,00270221	12	61
90S preribosome [GO:0030686]	0,0051299	13	74
fatty acid synthase complex [GO:0005835]	0,00633473	2	2
acetolactate synthase complex [GO:0005948]	0,00633473	2	2
anthranilate synthase complex [GO:0005950]	0,00633473	2	2
plasma membrane enriched fraction [GO:0001950]	0,00752225	14	86
mitochondrial proton-transporting ATP synthase complex [GO:0005753]	0,00837508	3	6

Tab S4

Click here to download Supplementary Material (for online publication): S4_tab.pdf

Upregulated genes >1.5

GO Molecular Function

Category	p-value	k	f
transporter activity [GO:0005215]	1,02E-005	15	90
substrate-specific transmembrane transporter activity [GO:0022891]	0,000374024	7	31
RNA polymerase II transcription factor binding transcription factor activity [GO:0001076]	0,00204395	2	2
alpha-glucoside:hydrogen symporter activity [GO:0005352]	0,00204395	2	2
glycerol transmembrane transporter activity [GO:0015168]	0,00204395	2	2
glucosidase activity [GO:0015926]	0,00280833	3	7
sequence-specific DNA binding [GO:0043565]	0,00313828	16	165
symporter activity [GO:0015293]	0,00434354	3	8
RNA polymerase II activating transcription factor binding [GO:0001102]	0,00594793	2	3

GO Cellular Component

Category	p-value	k	f
cellular_component [GO:0005575]	0,000394061	51	704
nuclear nucleosome [GO:0000788]	0,00105597	4	11
nucleosome [GO:0000786]	0,00105597	4	11
replication fork protection complex [GO:0031298]	0,00463078	5	25
ascospore wall [GO:0005619]	0,00869944	3	10

Tab S5

Click here to download Supplementary Material (for online publication): S5_tab.xlsx

S5_table List of differentially expressed genes

		Counts MUT1	Counts MUT2	Counts V	Counts WT2	baseMean
1	YPR053C	88	87	1887	1438	990.9536289
2	YBR072W	1118	1249	11381	11375	7115.939736
3	YOL058W	1187	1103	9989	9562	6158.364622
4	YPR052C	343	378	3121	2738	1846.010957
5	YDR344C	0	1	125	82	59.1514382
6	YER011W	506	514	5447	2904	2576.221761
7	YDL182W	5540	5554	32563	26622	19415.51843
8	YGR157W	1577	1439	8374	6896	5044.364843
9	YNL160W	4082	4403	22079	19371	13789.85012
10	YGR213C	741	786	3366	2872	2126.953264
11	YJL089W	128	113	574	531	371.6666365
12	YJR073C	1189	1229	5148	4756	3386.151131
13	YGR234W	2640	2531	11368	8850	6917.807149
14	YHL033C	5823	5693	24668	19222	15080.35301
15	YIL119C	96	132	512	437	322.5621742
16	YPR145C-A	42	34	201	156	118.8528175
17	YJL216C	375	427	1636	1228	993.3627449
18	YJL191W	1018	1158	4275	3260	2629.266276
19	YPL198W	1366	1553	5353	4078	3332.876027
20	YLL056C	795	769	2616	2110	1695.925361
21	YDR342C	6414	6370	21110	16564	13573.36609
22	YKL216W	2607	3071	8905	8010	6110.035452
23	YNL015W	766	761	2344	2187	1640.606835
24	YPL197C	193	220	740	548	457.7876177
25	YJL088W	126	108	446	316	268.270036
26	YNR050C	8432	8083	24064	21345	16673.65326
27	YGL089C	3107	3340	10793	7589	6640.771909
28	YBR056W-A	503	581	1606	1382	1095.051817
29	YDR534C	82	98	306	233	193.302987
30	YDR502C	3771	3890	11177	8825	7396.148116
31	YPR057W	436	493	1322	1087	893.300436
32	YBR177C	1581	1659	4470	3663	3038.212219
33	YNL040W	597	684	1734	1444	1190.922557
34	YOR120W	1787	1766	4465	4368	3328.2557
35	YNR034W-A	2154	2773	6520	6143	4727.060534
36	YHR015W	96	109	298	237	197.8668896
37	YBR040W	74	123	390	267	229.7848292
38	YHR022C	35	59	166	145	109.9264022
39	YER175C	623	552	1529	1331	1078.690834
40	YGL117W	971	932	2352	2178	1721.103572

Fig S1

Click here to download high resolution image

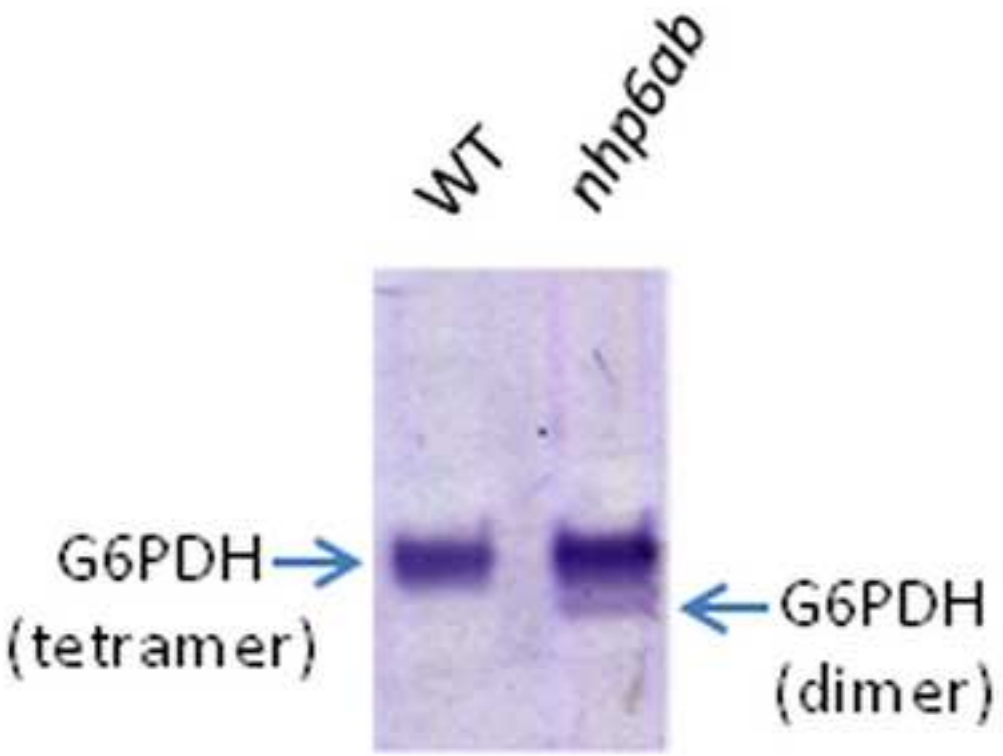

Fig S2
Click here to download high resolution image

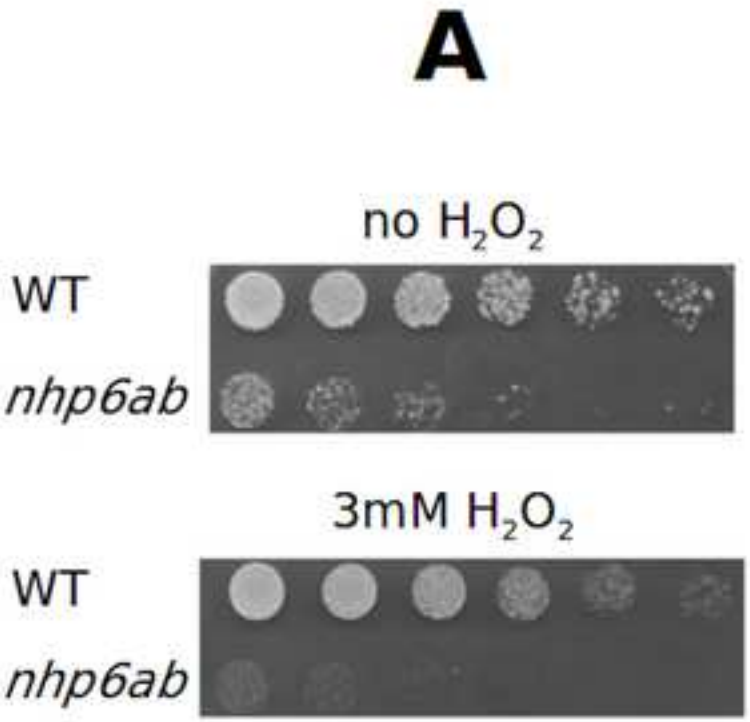

B

"stre" containing genes (95/195)
Expression nhp6ab/WT >1.2

ACH1 AHP1 APC1 APM3 ARA1 AST2 ATG3 ATG8 ATO3 AYR1 AZR1 BMH1 BOP3 CDC26 CLG1 COX5B CRF1 CWP1 DAL1 DIT1 ECM19 ECM7 EDE1 EMP24 FCP1 FLC2 FUN19 GAL2 GAL80 GLC3 GLK1 GPD1 GPI16 HOF1 HSP150 HSP33 HST2 HSV2 LSP1 MEK1 MIG2 MNN4 MOT1 MRPL15 MSC1 MSC3 MTL1 MYO1 NCE102 NET1 NTH1 NVJ1 PAI3 PDA1 PDI1 PHO91 PIB2 PIG2 PIL1 PMA2 PNS1 POR2 PRR2 PSY4 PTP2 PUT4 PXR1 ROD1 RPB4 RSM7 RTN1 SAL1 SDS24 SEC31 SGA1 SLM1 SLX8 SMC2 SNA2 SSM4 SUA5 TCM62 TDP1 TGL4 TPK1 TPS1 TPS2 TPS3 TUP1 TVP15 UBP15 ULA1 UTR4 XBP1 YAK1

Fig S3

Click here to download Supplementary Material (for online publication): Fig_S3.pdf

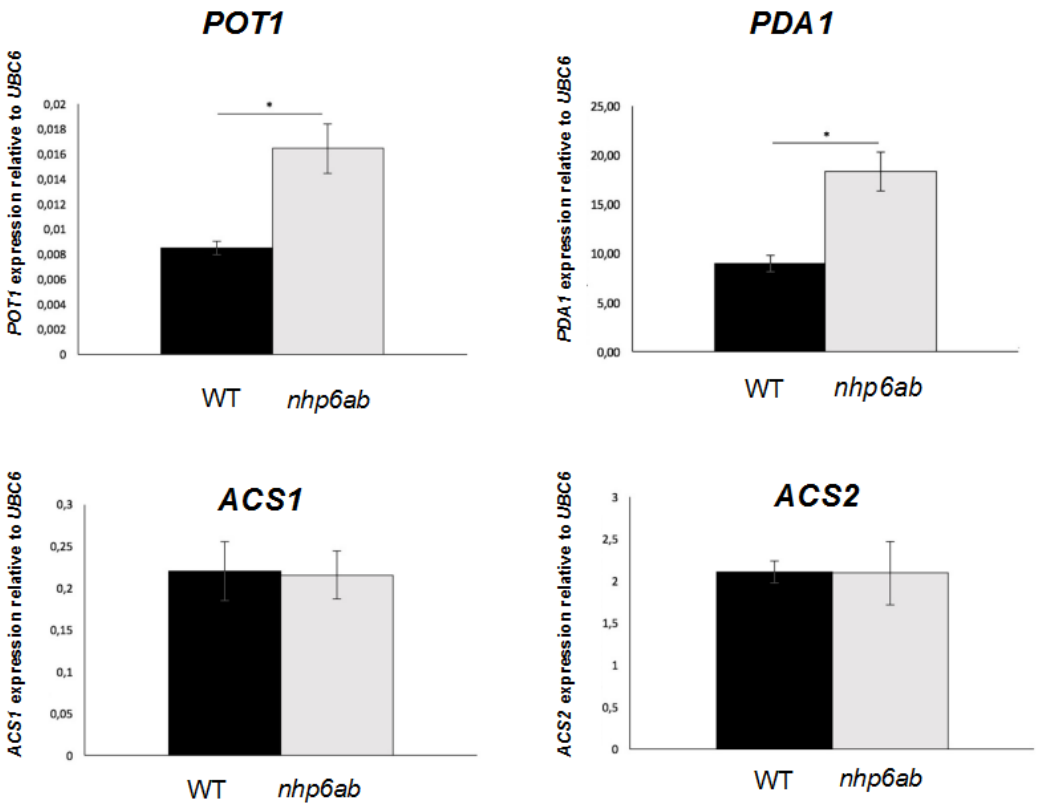

Supplementary Figure and tables captions

Click here to download Supplementary Material (for online publication): Supplementary Figures and Tables Captions.docx

Fig.S1 - G6PDH activity on native gel in WT and *nhp6ab* strains. Extracts from WT or *nhp6ab* cells grown on YPD medium (prepared as in 17), were separated on polyacrylamide gel and stained for G6PDH activities. $NADP^+$ and Glucose 6-P were used as cofactors and substrate for G6PDH activity. G6PDH tetrameric and dimeric forms are indicated (arrows).

Fig.S2 - A - Growth sensitivity to H_2O_2 treatment. WT or nhp6ab strains were grown on YPD medium to exponential phase (0.5 OD/ml). Cells were then treated or not with 3mM H_2O_2 for 30' at 30°C and aliquotes (45000 cells, serially diluted 1:3) were spotted on YPD plates and incubated for 3 days at 30°C. B - List of "stre" containing genes differentially expressed (>1.2 fold) between *nhp6ab* and WT.

Fig.S3 - *POT1, PDA1, ACS1* and *ACS2* expression profiles measured by RT-qPCR in WT and *nhp6ab* cells. (*) $p<0.05$ (T-student determined).

Table S1 - Resonance assigment

Table S2 - Intracellular metabolite concentrations expressed as means and Standard Deviation (SD) of µmol/g biomass weight. Unpaired data Student's t test was used to compare the differences.

Table S3 - Down regulated genes, GO Molecular Function

Table S4 - Upregulated genes, GO Molecular Function

Table S5 - List of differentially expressed genes